AD-779 799

FEASIBILITY STUDY OF EXOELECTRON IMAGING AS AN NDT METHOD FOR LASER SURFACE DAMAGE OF NONLINEAR OPTICAL MATERIALS AND LASER GLASS

Peter F. Braunlich, et al

Bendix Research Laboratories

Prepared for:

Air Force Cambridge Research Laboratories

September 1973

UNCLASSIFIED

Security Classification

AD 779 799

DOCUMENT CONTROL DATA - R&D

(Security classification of title, body of abstract and indexing annotation must be entered when the overall report is classified)

1. ORIGINATING ACTIVITY (Corporate author)
Bendix Research Laboratories
Bendix Center
Southfield, Michigan 48076

2a. REPORT SECURITY CLASSIFICATION
Unclassified

2b. GROUP

3. REPORT TITLE
FEASIBILITY STUDY OF EXOELECTRON IMAGING AS AN NDT METHOD FOR LASER SURFACE DAMAGE OF NONLINEAR OPTICAL MATERIALS AND LASER GLASS

4. DESCRIPTIVE NOTES (Type of report and inclusive dates)
Scientific. Interim. (March - September 1973)

5. AUTHOR(S) (Last name, first name, initial)
Peter F. Braunlich
John P. Carrico

6. REPORT DATE	7a. TOTAL NO. OF PAGES	7b. NO. OF REFS
September 1973	82	15

8a. CONTRACT OR GRANT NO.
F19628-73-C-0032

b. PROJECT NO. Task, Work Unit Nos.
2042 n/a n/a

c. Dod Element 62701E

d. DoD Subelement n/a

9a. ORIGINATOR'S REPORT NUMBER(S)
Semi-Annual Technical Report No. 2
BRL Report 7058

9b. OTHER REPORT NO(S) (Any other numbers that may be assigned this report)
AFCRL-TR-73-0591

10. AVAILABILITY/LIMITATION NOTICES
A - Approved for public release; distribution unlimited.

11. SUPPLEMENTARY NOTES
This research was sponsored by the Defense Advanced Research Projects Agency.

12. SPONSORING MILITARY ACTIVITY
Air Force Cambridge Research Labs (LQ)
L. G. Hanscom Field
Bedford, Massachusetts 01730

13. ABSTRACT

This semi-annual report presents the results of a second six-month effort on the development of an NDT method to predict laser surface damage on dielectric materials used in high power laser systems.

Experimental results on thermally and/or optically stimulated exoelectron emission from Nd-2 laser glass, and NaCl and $LiNbO_3$ single crystals after electron bombardment or exposure to high peak power laser pulses are given. Computer calculations of the spatial variation of the density of trapped electrons after exposure of a pure NaCl single crystal to a high peak power pulse of a TEM_{00} mode laser beam are reported and discussed. Experiments on exoelectron images from LiF surfaces are interpreted on the basis of these results. The role of a white-hot plasma in front of the examined LiF surface is described. New information on multiphoton free carrier generation, on free carrier absorption, and on their involvement in the exoelectron processes and in the surface damage mechanisms was obtained.

DD FORM 1 JAN 64 1473

UNCLASSIFIED

Security Classification

14. KEY WORDS	LINK A		LINK B		LINK C	
	ROLE	WT	ROLE	WT	ROLE	WT
Pyroelectric materials						
Laser surface damage threshold						
$LiNbO_3$						
Laser glass						
Thermally stimulated field emission						
Exoelectron emission						
Laser optical materials						
Dielectric materials						

INSTRUCTIONS

1. ORIGINATING ACTIVITY: Enter the name and address of the contractor, subcontractor, grantee, Department of Defense activity or other organization *(corporate author)* issuing the report.

2a. REPORT SECURITY CLASSIFICATION: Enter the overall security classification of the report. Indicate whether "Restricted Data" is included. Marking is to be in accordance with appropriate security regulations.

2b. GROUP: Automatic downgrading is specified in DoD Directive 5200.10 and Armed Forces Industrial Manual. Enter the group number. Also, when applicable, show that optional markings have been used for Group 3 and Group 4 as authorized.

3. REPORT TITLE: Enter the complete report title in all capital letters. Titles in all cases should be unclassified. If a meaningful title cannot be selected without classification, show title classification in all capitals in parenthesis immediately following the title.

4. DESCRIPTIVE NOTES: If appropriate, enter the type of report, e.g., interim, progress, summary, annual, or final. Give the inclusive dates when a specific reporting period is covered.

5. AUTHOR(S): Enter the name(s) of author(s) as shown on or in the report. Enter last name, first name, middle initial. If military, show rank and branch of service. The name of the principal author is an absolute minimum requirement.

6. REPORT DATE: Enter the date of the report as day, month, year; or month, year. If more than one date appears on the report, use date of publication.

7a. TOTAL NUMBER OF PAGES: The total page count should follow normal pagination procedures, i.e., enter the number of pages containing information.

7b. NUMBER OF REFERENCES: Enter the total number of references cited in the report.

8a. CONTRACT OR GRANT NUMBER: If appropriate, enter the applicable number of the contract or grant under which the report was written.

8b, 8c, & 8d. PROJECT NUMBER: Enter the appropriate military department identification, such as project number, subproject number, system numbers, task number, etc.

9a. ORIGINATOR'S REPORT NUMBER(S): Enter the official report number by which the document will be identified and controlled by the originating activity. This number must be unique to this report.

9b. OTHER REPORT NUMBER(S): If the report has been assigned any other report numbers *(either by the originator or by the sponsor)*, also enter this number(s).

10. AVAILABILITY/LIMITATION NOTICES: Enter any limitations on further dissemination of the report, other than those imposed by security classification, using standard statements such as:

(1) "Qualified requesters may obtain copies of this report from DDC."

(2) "Foreign announcement and dissemination of this report by DDC is not authorized."

(3) "U. S. Government agencies may obtain copies of this report directly from DDC. Other qualified DDC users shall request through _____."

(4) "U. S. military agencies may obtain copies of this report directly from DDC. Other qualified users shall request through _____."

(5) "All distribution of this report is controlled. Qualified DDC users shall request through _____."

If the report has been furnished to the Office of Technical Services, Department of Commerce, for sale to the public, indicate this fact and enter the price, if known.

11. SUPPLEMENTARY NOTES: Use for additional explanatory notes.

12. SPONSORING MILITARY ACTIVITY: Enter the name of the departmental project office or laboratory sponsoring *(paying for)* the research and development. Include address.

13. ABSTRACT: Enter an abstract giving a brief and factual summary of the document indicative of the report, even though it may also appear elsewhere in the body of the technical report. If additional space is required, a continuation sheet shall be attached.

It is highly desirable that the abstract of classified reports be unclassified. Each paragraph of the abstract shall end with an indication of the military security classification of the information in the paragraph, represented as *(TS)*, *(S)*, *(C)*, or *(U)*.

There is no limitation on the length of the abstract. However, the suggested length is from 150 to 225 words.

14. KEY WORDS: Key words are technically meaningful terms or short phrases that characterize a report and may be used as index entries for cataloging the report. Key words must be selected so that no security classification is required. Identifiers, such as equipment model designation, trade name, military project code name, geographic location, may be used as key words but will be followed by an indication of technical context. The assignment of links, rules, and weights is optional.

AFCRL – TR-73-0591

FEASIBILITY STUDY OF EXOELECTRON IMAGING AS AN NDT METHOD FOR LASER SURFACE DAMAGE OF NONLINEAR OPTICAL MATERIALS AND LASER GLASS

by
Peter F. Braunlich and John P. Carrico
Bendix Research Laboratories
Bendix Center
Southfield, Michigan 48076

Contract No. F19628-73-C-0032
Project No. 2042

Semi-Annual Technical Report No. 2

September 1973

Contract Monitor: John V. Nikula
Solid State Sciences Laboratory

Sponsored by
Defense Advanced Research Projects Agency
ARPA Order No. 2042

Monitored by
AIR FORCE CAMBRIDGE RESEARCH LABORATORIES
AIR FORCE SYSTEMS COMMAND
UNITED STATES AIR FORCE
BEDFORD, MASSACHUSETTS 01730

ARPA Order No. 2042

Program Code No. 2D1

Contractor: Bendix Research Laboratories

Effective Date of Contract: 15 August 1972

Contract No. F19628-73-C-0032

Principal Investigator and Phone Number: Dr. Peter F. Braunlich
(313) 352-7725

AFCRL Project Scientist and Phone Number: John V. Nikula
(617) 861-3532

Contract Expiration Date: 14 February 1974

Previous Contract Report: Semi-Annual Report No. 1
March 1973

Related Project: Exoelectron Study of Surface Damage of Laser Materials, performed under Subcontract to Wayne State University, under National Science Foundation Contract GH-32606

TABLE OF CONTENTS

LIST OF ILLUSTRATIONS

SECTION 1
INTRODUCTION

The present research effort has been based on the observation[1] of a characteristic exoelectron image of an optical quality LiF single crystal after its exposure to a 50 ns pulse of about 15 J/cm^2 from a Nd-glass laser. This was the first time that exoelectron emission was observed from a dielectric material after exposure to intense laser light. The initially proposed[1] theoretical explanation for this imaging was multi-photon photocarrier generation and subsequent trapping of a part of these carriers in electron traps. An apparent relation between these electronic processes and the precursors of laser damage was then taken as the basis for the present research program. The scope of this program, as described in the first semi-annual report (AFCRL-TR-73-0068, March 1973), is to determine the feasibility of using exoelectron surface imaging as an NDT method of predicting the laser surface damage threshold for laser optical materials.

During the present reporting period, we performed computer calculations of the processes leading to exoelectron image formation in pure NaCl containing F-centers (traps). This work is described in Section 2. The basis for this work is the multiphoton mechanism mentioned above. A major result of the NaCl calculations is the conclusion that a similar mechanism cannot be responsible for the exoelectron images observed in LiF. In search of an alternate mechanism, we then experimented on LiF single crystals (Section 3). These experiments clearly demonstrate that the occurrence of a spark or plasma close to the sample surface is responsible both for filling traps with electrons and for forming the observed exoelectron images. This is not to say that multiphoton processes will not lead to exoelectron images under any circumstances. They will, however, require a much higher photon flux than that which can be tolerated by the optical quality LiF samples we used so far. A detailed discussion of this whole question is given in Section 3.

Experimental work has also proceeded on thermally and optically stimulated electron emission from selected laser materials. This work, which is reported in Section 4, resulted in the discovery of several interesting new phenomena and shows the need for improved control of surface conditions. The progress made on developing a new exoelectron emission microscope is reported in Section 5.

SECTION 2

APPLICATION OF THEORY TO EXOELECTRON EMISSION FROM NaCl

2.1 THEORY

2.1.1 Rate Equations

We have undertaken the development of a detailed theory of laser-induced exoelectron emission from optical materials in order to gain further insight into the processes responsible for the formation of the observed[1] exoelectron images. An outline of this theory was presented in the first semi-annual report (AFCRL-73-0068, March 1973). In this section, we report on the application of this theory to NaCl which is exposed to high power ruby laser pulses. We first determine the density of trapped electrons as a function of laser flux. In turn, this information together with the known intensity profile of the laser beam can be converted into a spatial distribution for the trapped electron density. A correlation between this spatial distribution and the observed exoelectron images should then be possible.

NaCl was chosen because its properties are well known[2] and all the parameters (cross sections for multiphoton absorption and electron trapping, transition probabilities, etc.) are either known from independent experiments or can be calculated. We consider a pure NaCl crystal containing a given natural density of ion-vacancies. The Cl^- vacancy forms an F-center upon capture of a free electron. This center is the electron trap. During the laser pulse, free carriers are generated and some of them are trapped in the Cl^- vacancies. The wavelength (λ = 6943Å) of the ruby laser corresponds to a quantum energy of 1.78 eV. Therefore, NaCl, having a band gap E_g = 8.1 eV, requires a five-photon absorption process for free carrier generation.

The physical processes which are responsible for the spatial distribution of trapped electrons can be described by equations (8) and (9) in the first semi-annual report, appropriately modified for NaCl. For

convenience, we repeat these equations; hereafter they will be referred to as equations (1) and (2), respectively:

$$\frac{dn_c}{dt} = n_c \omega_i + n_v \omega_{vc} + n_t \omega_{tc} - n_c (n_c + n_t) \omega_{cv} - n_c (N_t - n_t) \omega_{ct} \quad (1)$$

$$\frac{dn_t}{dt} = n_v (N_t - n_t) \omega_{vt} + n_c (N - n_t) \omega_{ct} - n_t (n_c + n_t) \omega_{tv} - n_t \omega_{tc} \quad (2)$$

The assumptions leading to these equations and the specific notation are discussed in the first semi-annual report. The modifications for NaCl are:

- Consider the excited level of the F-center in addition to the F-center ground level because, according to Markham,[2] the retrapping traffic toward the ground-state of the F-center occurs via the excited level. As a result, we had to change the notation slightly. For convenience, the notation used in this section is listed below.
- Replace the term $(n_c + n_t) \omega_{cv}$ in equation (1) by the lifetime τ_c of the free carriers.
- Neglect the transition probability ω_{vt} for the valence electron to reach Cl^- vacancies directly.
- Add an equation for the temperature change of the sample during and after laser exposure.

A schematic of the energy level diagram for NaCl containing F-centers and the relevant transitions is shown in Figure 1.

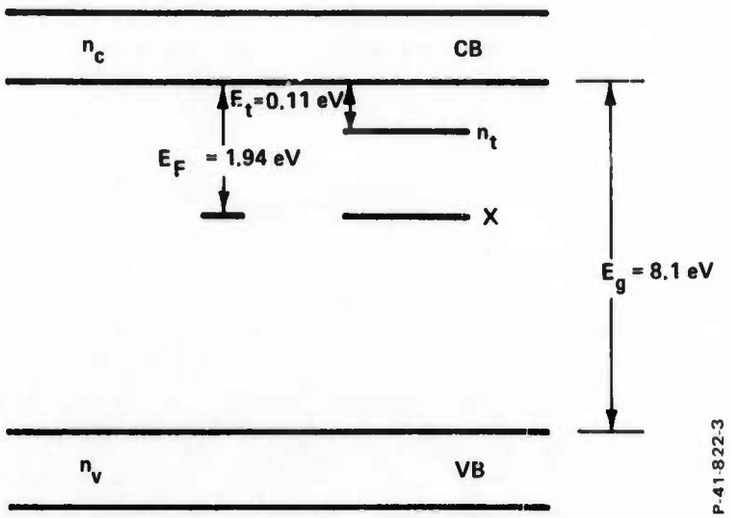

ENERGY LEVEL DIAGRAM FOR NaCl

Figure 1 - Energy level diagram of NaCl

2.1.2 Notation

N = density of Cl^- vacancies

$\dot{X}$ = density of F-centers in ground state

n_t = density of F-centers in excited state

n_c = density of free electrons in the conduction band (cb)

n_v = density of valence electrons

ω_i = ionization rate

ω_{vc} = transition probability for 5-photon photocarrier generation

ω_{ct} = transition probability for electron capture into the excited F-center level

ω_{tc} = transition probability for electrons to go from the excited F-center level to the conduction band

τ_c = lifetime of conduction electrons

τ_t = lifetime of electrons in excited F-center levels

ω_{Fc} = transition probability for electrons to go from the ground level of the F-center to the conduction band

T = temperature

W = absorbed energy density

ρ = density of crystal

κ = specific heat of the crystal

t_p = laser pulse width (FWHM)

τ_i = electron-phonon collision time

$\Delta\omega$ = width of F-band = $\frac{0.46 \text{ eV}}{\hbar}$

t = time

E = trap depth (in general)

F = laser photon flux

A* = laser peak flux

E_g = 8.1 eV = bandgap of NaCl

E_F = 1.94 eV = energy difference between F-center ground level and lower edge of the conduction band in NaCl[2]

E_t = 0.11 eV = energy difference between excited level of F-center and lower edge of the conduction band in NaCl[2]

λ = 6943Å = wavelength of ruby light

$\mu = \frac{\omega}{2\pi} = (2\pi)^{-1} \times 2.63 \times 10^{15} \text{ s}^{-1}$ = frequency of ruby laser light (the corresponding quantum energy is 1.78 eV)

r = distance from center of the laser beam

σ_5 = generalized cross section for five-photon absorption in NaCl

σ_1 = cross section for single-photon absorption by an electron in the excited level of an F-center

σ_2 = two-photon absorption cross section for ground state F-center

E_o = rms field strength of laser photon field

The relevant equations to be solved are then:

$$\frac{dn_c}{dt} = n_v \omega_{vc} - n_c/\tau_c + n_t \omega_{tc} - n_c (N - X - n) \omega_{ct} + \omega_{Fc} X + \omega_i n_c \quad (3)$$

$$\frac{dn_t}{dt} = -n_t \omega_{tc} + n_c (N - X - n_t) \omega_{ct} - n_t/\tau_t \quad (4)$$

$$\frac{dX}{dt} = -\omega_{Fc} X + n_c/\tau_t \quad (5)$$

and

$$\frac{dT}{dt} = (\rho\kappa)^{-1} \frac{dW}{dt} \quad (6)$$

2.1.3 Calculation of Parameters

We will now determine all the relevant parameters needed to numerically solve the rate equations (3) through (6).

The transition probability ω_{vc} for the five-photon absorption process is $\omega_{vc} = \sigma_5 F^5$. The generalized absorption cross section $\sigma_5 = 0.5 \times 10^{-140} cm^{10} s^4$ was measured by Catalano and coworkers[3] and agrees reasonably well with theoretical calculations.[4] From the molecular weight of 58.44g and the density $\rho = 2.165$ g/cm^3, the density of active atoms (Cl^- atoms) is calculated to be $n_v = 2.23 \times 10^{22}/cm^{-3}$. Therefore, the 5-photon generation rate $n_v \omega_{vc} = 1.12 \times 10^{-118} F^5$ (measured in s^{-1}).

The time dependence of the laser pulse (photon flux) is, in fair approximation to the actual pulse shape,

$$F = A^* \sin^2\left(\frac{\pi t}{2t_p}\right)$$

measured in photons/cm^2-s. The probability $\omega_{tc} = \omega_{tc}^{th} + \omega_{tc}^{o}$ contains the thermal transition probability

$$\omega_{tc}^{th} = v_{th} N_c \sigma e^{-E_t/kT}$$

and the probability ω_{tc}^{o} for single photon absorption by electrons in the excited level of the F-center.

The effective density of states[2] at the lower edge of the conduction band is

$$N_c = 2\left(\frac{2\pi m^* k}{h^2}\right)^{3/2} T^{3/2} = 4.8 \times 10^{15}\ T^{3/2}\ (cm^{-3}),$$

assuming that the effective mass m* of the conduction electron is equal to the free electron mass. The thermal velocity

$$v_{th} = (3\ kT/m^*)^{1/2}$$

The probability of electron capture into the excited state of the F-center[2] is about 10^{-13} cm^2; therefore,

$$\omega_{tc}^{th} \sim 7 \times 10^{9}\ T^{3/2}\ e^{-0.11\ eV/kT}.$$

Since

$$\omega_{ct} = \omega_{tc}^{th} N_c\ e^{-0.11\ eV/kT}$$

we find $\omega_{ct} = 1.45 \times 10^{-6}$ $(cm^3\ s^{-1})$. The probability for single photon absorption is

$$\omega_{tc}^{o} = \sigma_1 F = \frac{2}{9} \frac{e^2}{m^* c} \frac{f}{\Delta\nu} \frac{\left(2 + n_r^2\right)^2}{n_r}$$

where $n_r = 1.53$ is the refractive index of NaCl at 6943Å, $f \approx 1$ the oscillator strength of the transition, and $\Delta\nu \approx 0.5\nu$ its line width. The cross section then becomes, in our case, $\sigma_1 = 1.1 \times 10^{-16}$ cm^2. In a similar way, we calculated the cross section σ_2 for the two-photon transition from the ground state of the F-center to the conduction band. We have

$$\omega_{Fc} = \omega_{Fc}^{o} + \omega_{Fc}^{th} \text{ and } \omega_{Fc}^{o} = \sigma_2 F.$$

According to Kleinman,[5]

$$\sigma_2 = \frac{r_o^2 \, 8\pi^3 \, c^2 \, f^2}{n_r^2 \, \omega^2 \, \Delta\omega} F.$$

Here $r_o = 2.82 \times 10^{-13}$ cm is the classical electron radius, c the velocity of light, $\omega(\text{ruby}) = 2.63 \times 10^{15}$ s^{-1}, and f is an average of the involved oscillator strengths.

With[2]

$$\Delta\omega = \frac{0.46}{\hbar} \text{ eV} = 0.68 \times 10^{15} \text{ s}^{-1}$$

and using $f = 1$, we obtain $\omega_{Fc}^{o} = 1.6 \times 10^{-48} F^2$ (s^{-1}). The thermal part of ω_{Fc} can be estimated. We know that the cross section for electron capture into the ground state of the F-center is about two orders of magnitude smaller than that for capture into the excited state;[2] furthermore, it decreases with temperature. Assuming the cross section for capture into the F-center ground state is only one-tenth of that for

capture into the excited state, we obtain

$$\omega_{Fc}^{th} = 7 \times 10^{8}\ T^{3/2}\ e^{-E_F/kT}$$

Admittedly, ω_{Fc}^{th} might be slightly overestimated; however, measurements of it, based on thermally stimulated processes, are less reliable in light of recent investigations.[6,7] This thermal transition influences the degree of trap filling after the laser pulse if the temperature increases to several hundred degrees centigrade. A more accurate value is desired; achieving this is one of the goals of our investigations. However, for the actual damage process (see below), this transition is rather insignificant.

Equation (6) is derived from

$$\frac{dW}{dt} = n_c \frac{e^2\ \tau_i\ E^2}{m^* \left(1 + \tau_i^2\ \omega^2\right)}$$

the rate of energy absorption per cm^3 due to free carrier absorption of laser photons.[8,9] Here $\tau_i = 0.5 \times 10^{-15}$ s (electron-phonon collision time),[10] and E is the rms-value of the optical field strength which is obtained[8] from

$$E^2 = \frac{4\pi\ F\ \varkappa\ \omega}{c\ n_r}$$

In accordance with Hellwarth,[11] we assume now that the electrons transfer the absorbed energy to the lattice in a time that is fast compared to the laser pulse width t_p. This enables us to calculate the temperature increase from

$$\frac{dT}{dt} = \frac{1}{\rho\kappa}\frac{dW}{dt} = 2.7 \times 10^{-20}\ n_c\ E_o^2\ \text{(deg/s)}$$

where E_o is measured in V/cm, or

$$\frac{dT}{dt} = 1.9 \times 10^{-36} \, n_c \, F \text{ (ruby)}$$

where we used the value $\kappa = 0.203$ cal/g-deg for the specific heat of NaCl.

2.2 NUMERICAL CALCULATIONS

2.2.1 Method

The numerical calculations of equations (3) through (6) were performed using a modified Runge-Kutta method with variable step size. We have, in a first approximation, neglected the temperature rise of the sample. Numerical estimates show that this assumption does not affect the obtained results up to photon fluxes $A^* \lesssim 3 \times 10^{28}$ cm^{-2} s^{-1}. The damage threshold for NaCl was determined by Bloembergen's group[9,10,12] to be 2.1×10^6 V/cm = 6.9×10^{28} photons/cm^2-s. At fluxes larger than about 4×10^{28} cm^{-2} s^{-1}, the temperature increases dramatically. This increase could constitute an alternative damage mechanism to dielectric breakdown, the mechanism advocated by Bloembergen et al. This is discussed in more detail in the next section.

Since the lifetime of free carriers[3] is 10^{-6} s and the lifetime of the excited F-center[2] is also 10^{-6} s, no significant loss of photocarriers occurs during the 30 ns laser pulse. Thereafter, the photocarriers decay with a lifetime of 10^{-6} s and the excited F-centers relax to the ground level, thus filling the traps. This population of filled traps acts as the reservoir for exoelectrons which are observed during the thermally stimulated exoelectron experiment. Because these lifetimes are relatively long compared to the laser pulse duration ($\sim$50 ns), we are thus able to perform the calculations in two steps. The first corresponds to the process in which the NaCl is excited by the laser pulse. For this case, the relevant time domain for solving the differential equations (3) through (6) is $0 = t \leq t_p$ and we neglect

terms proportional to τ_c and τ_t. The second step of the calculations corresponds to the relaxation of the NaCl after the laser pulse. In this step, we neglect all terms in equations (3) through (6) that contain the laser flux F. The redistribution of all electrons then occurs via the decay of conduction electrons to the valence band and the decay of the electrons in the excited level to the ground level of the F-center.

We have solved equations (3) through (6) first without considering avalanche ionization ($\omega_i \equiv 0$), in order to find out whether the Hellwarth mechanism[11] can account for the damage. Hellwarth contends that the conduction electrons deposit their energy (e.g., absorbed from the laser photon field by inverse Bremsstrahlung) in the lattice before they reach sufficient kinetic energy for lattice ionization. In addition, exoelectron images might be formed by depositing electrons in Cl^- vacancies before avalanche sets in.

2.2.2 Results of Numerical Calculations

The following initial conditions were used

- $N = 5 \times 10^{16}$ cm^{-3}; Cl^- vacancies/cm^3
- $X = 5 \times 10^{15}$ cm^{-3}; initially filled traps (F-centers) due to, e.g., pre-radiation with X-rays
- $n_c(o) = n_t(o) = 0$
- $T = 300°K$

We calculated first the densities $n_c(2t_p)$, $n_t(2t_p)$, and $X(2t_p)$ for $t_p = 30$ ns and $F = A^* \sin^2 [\pi t/(2t_p)]$. The laser pulse ends at $t = 2t_p$, and t_p is the FWHM-value of the pulse. The results are shown in Figure 2. All numbers are normalized to 5×10^{16} cm^{-3}, the initial density of the Cl^- vacancies.

The density of filled traps (F-centers) at $t = 2t_p$ decreases sharply with increasing peak flux A*. All initially available F-centers are converted back to Cl^- vacancies at $A^* > 10^{28}$ photons/cm^2-s. Of course, this is to be expected, because the refilling mechanism (decay of excited F-centers to ground state) is not yet operative at 60 ns, and two-photon absorption excites the electrons from the ground-state F-centers into the

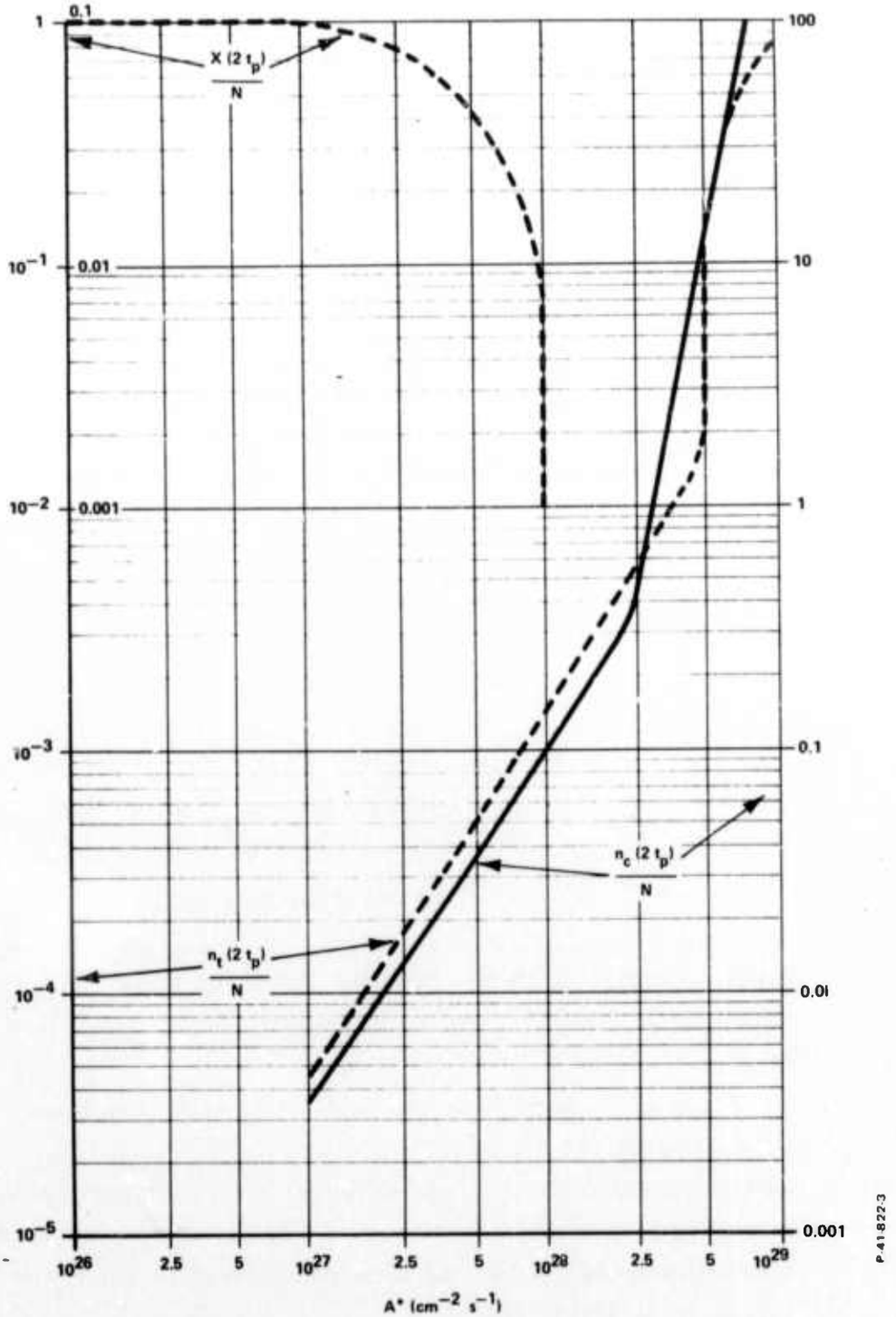

Figure 2 - Normalized densities of F-centers in the ground state (X/N), of conduction electrons (n_c/N), and of electrons in the excited level of the F-center (n_t/N) at time $t = 2t_p$ (the end of the laser pulse) as a function of the peak photon flux A*.

conduction band. The increase in both n_c and n_t is initially proportional to $(A^*)^{3/2}$. The increase in the density of conduction electrons then becomes proportional to $(A^*)^5$ due to 5-photon free carrier generation. At $A^* \sim 5 \times 10^{28}$ cm^{-2} s^{-1}, n_t increases sharply and eventually merges into saturation at large fluxes where $n_t(2t_p) = N$, the condition that all F-centers are in the excited state.

After the laser pulse, at $t \geq 2t_p$, the densities n_c and n_t decrease exponentially with a time constant of $\tau = 10^{-6}$ s. Of interest now is the behavior of $X(t > 2t_p)$. Refilling of the traps via the decay of n_t now replenishes electrons lost by two-photon absorption of the F-centers. This is shown in Figure 3 where $X(2t_p + 6\tau_c)$ is plotted as a function of the peak flux of the laser pulse. At $A^* \approx 10^{28}$ cm^{-2} s^{-1}, X reaches a minimum and increases thereafter, asymptotically approaching 5×10^{16} cm^{-3} (the density of Cl^- vacancies) at high photon fluxes.

The spatial variation of the density of F-centers along the sample surface is obtained from the results of Figure 3 by employing the intensity profile of the laser beam to convert the dependence of X on A* into a function of r, the distance from the center of the laser beam. Assuming this beam profile to be a Gaussian with a minimum spot size of 2 mm diameter, we obtain, not surprisingly, the profile of the F-center density distribution of the exoelectron image shown in Figure 4. One can clearly distinguish three different intensity zones:

- Bleaching of F-centers due to two-photon absorption at low flux A* - Region I
- Refilling of F-centers due to decay of n_t after the laser pulse - Region II
- Center region which is bleached again due to a rise in temperature (note that the dashed curve is not corrected for temperature effects and this latter bleaching effect is not shown in Figure 4). - Region III

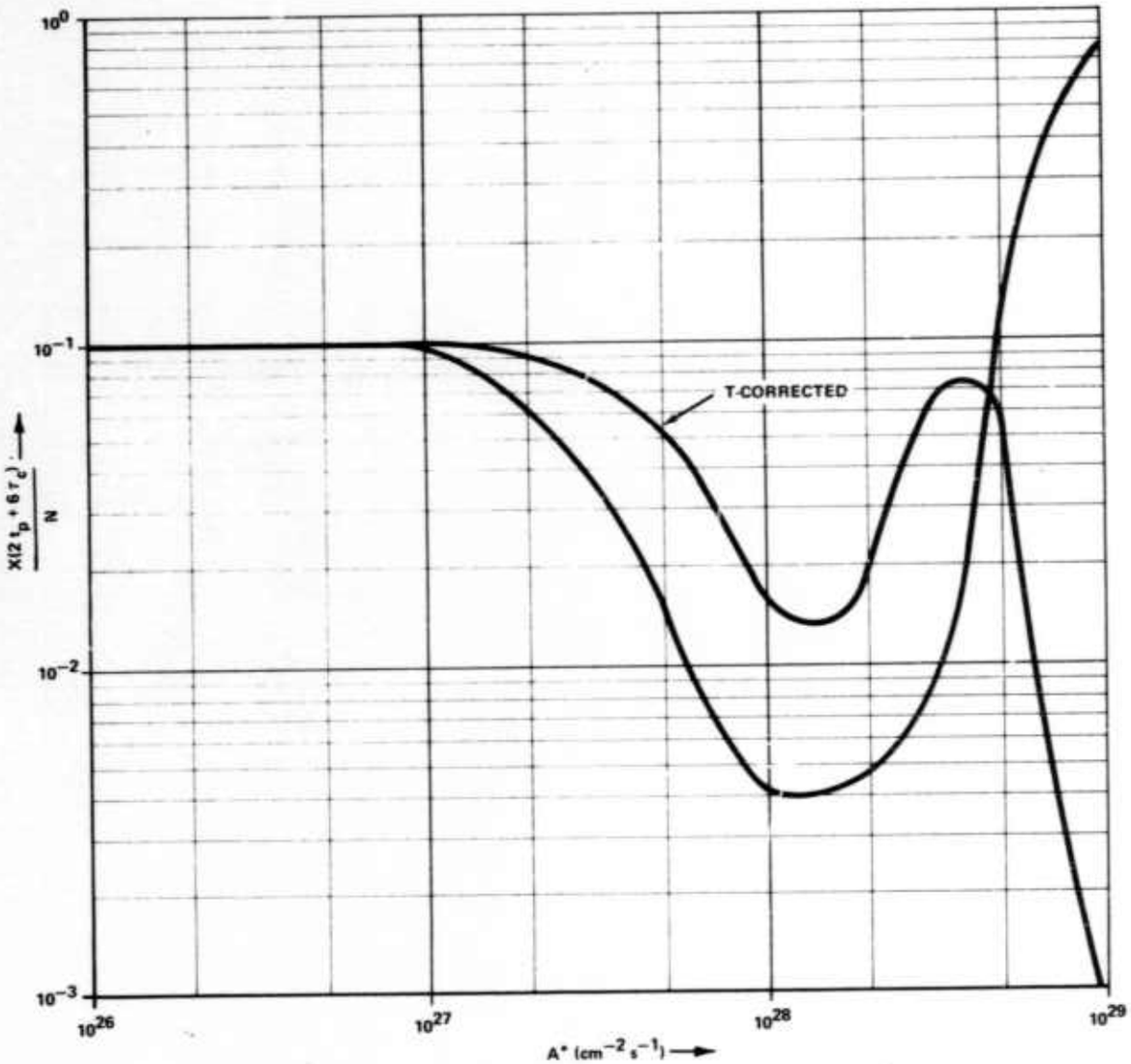

Figure 3 - Normalized density of F-centers in the ground state after long decay (six decay constants) of both the conduction electrons and the electrons in the excited F-centers as a function of the peak photon flux A*. This density is the density of electrons that remain trapped after the exposure of the NaCl crystal to an intense laser pulse.

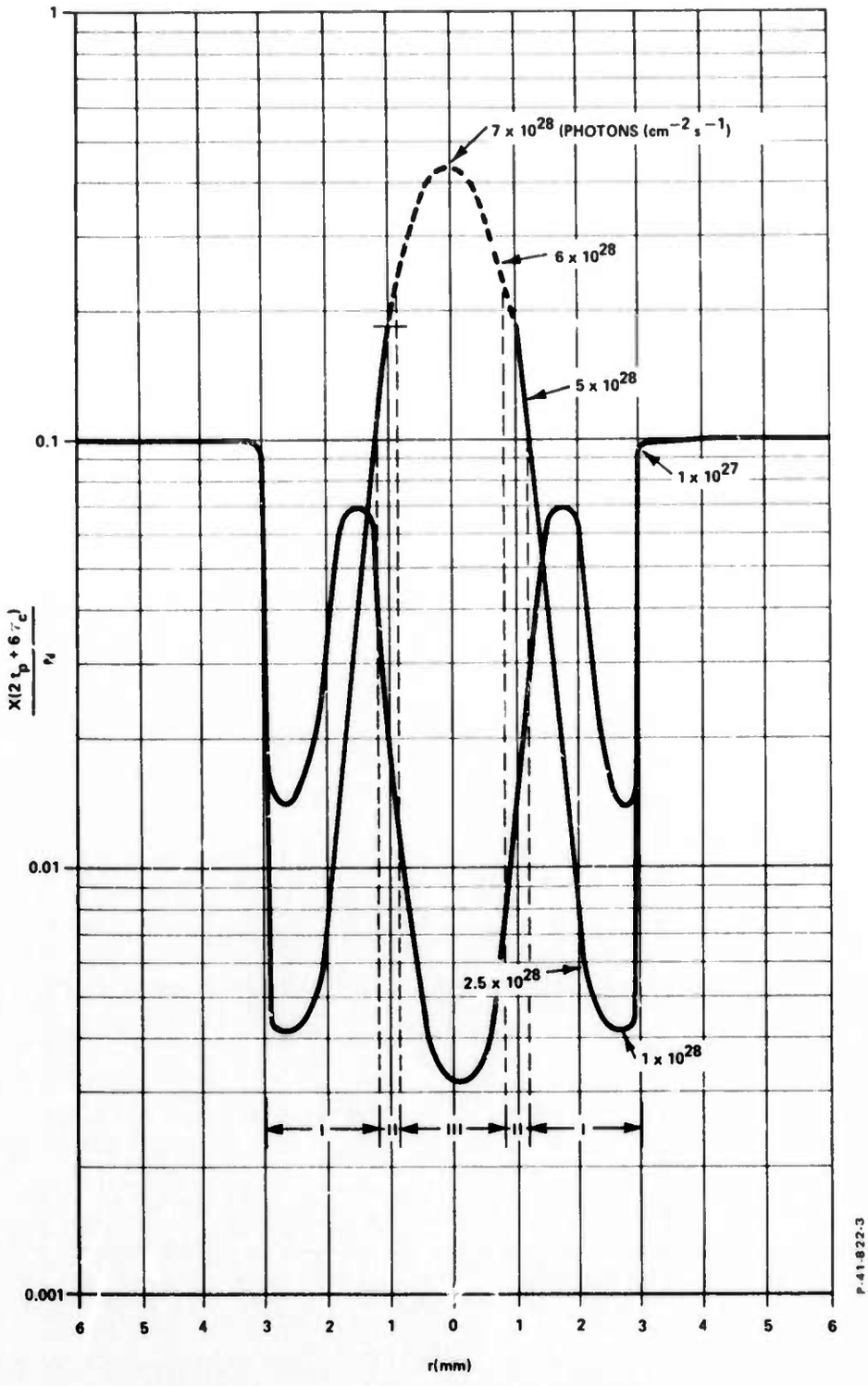

Figure 4 - Spatial variation of the density of trapped electrons as a function of the radial distance from the center of the laser intensity profile. The intensity profile of a mode TEM_{00} laser pulse with a minimum spot size of 2 mm was used to convert the data shown in Figure 3 to this diagram. The arrows indicate the peak photon flux A* of the corresponding laser intensity profile.

The rise in temperature, given by equation (6) is of considerable interest. Up to this time, we have not included this rise in our computer calculations; however, an estimate of the temperature increase can be obtained quite easily. Equation (6), as applied to NaCl and a ruby laser beam, reads $dT = 1.9 \times 10^{-36} F n_c dt$. We assume that, on the average, F can be replaced by A*/2 and

$$\int_0^{2t_p} n_c \approx n_c (2t_p) t_p/2$$

This results in the temperature increase

$$\Delta T = 0.95 \times 10^{-36} A^* n_c t_p^2$$

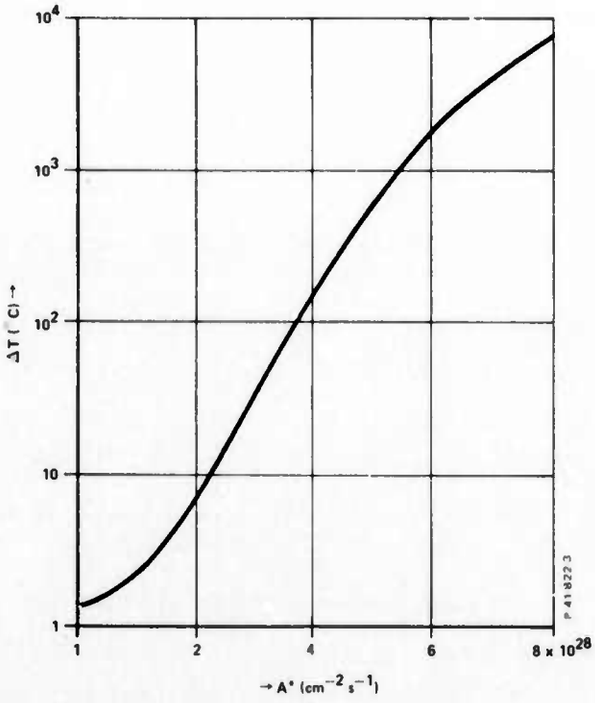

Figure 5 - Estimation of the temperature increase ΔT of the sample at $t = 2t_p$ (end of the laser pulse) as a function of peak laser flux A*.

shown in Figure 5. Of course, since some of the transition probabilities in equations (3) through (6) are temperature dependent, this is not expected to be a very good approximation. It is, however, sufficient to obtain a first impression of the temperature effects that take place even in the absence of avalanche ionization; the latter sets in a 7×10^{28} photons/cm^2-s for a 30 ns pulse of a ruby laser.[11,12]

Two comments concerning the preceding calculations are in order:

- The rapid rise of the temperature at photon fluxes of more than about 4×10^{28} cm^{-2} s^{-1} can conceivably cause damage without the assumption of an avalanche mechanism (the so-called Hellwarth mechanism).
- The high temperatures that can be reached even before damage sets in require the addition of a thermal diffusion term in equation (6) and the discussion of its influence on the occupation of the traps at times $t >> 2t_p$ and, therefore, on the exoelectron image as well.

SECTION 3
LiF INVESTIGATIONS

Calculations similar to those described in the previous section have not been carried out for LiF as of now. The main reason for this is the lack of data on the relevant cross sections and transition probabilities. We are able, however, to discuss the effects measured in LiF on the basis of the NaCl calculations. From the ratio $E_{Br}(LiF)/E_{Br}(NaCl) = 2.67$, measured by Vorobev et al.[13] for dc fields and from the theory for optical breakdown of alkali halides,[9] we conclude that the breakdown field strength from LiF must be about 5.6×10^6 V/cm at the frequency of the ruby laser. This value corresponds to 4×10^{29} photons cm^{-2} s^{-1}. Since the process of photocarrier generation in LiF by absorption of ruby photons is 7-photon absorption, we expect the cross section for this process to be much smaller than the cross section for 5-photon absorption in NaCl. Therefore, the processes that are expected to lead to exoelectron images after exposure of LiF to pulses of a ruby laser will occur at fluxes that are considerably higher than those calculated for NaCl.

Previous experiments[1] on exoelectron images after exposure to a Nd-laser pulse indicated, however, that the damage threshold was about 15 J/cm^2 for 50 ns pulses. Recent experiments using the Owens-Illinois single TEM_{00} mode Nd-glass laser confirmed the results. The damage threshold of optical quality LiF crystals, supplied by Harshaw Chemical, was determined to be 20 J/cm^2. This corresponds to 2.3×10^{27} photons cm^{-2} s^{-1} or 3×10^5 V/cm. Damage occurs, therefore, in the examined LiF samples at a fraction of the expected rms electric field strength. We conclude from this that the damage threshold measured for these LiF samples was not the "natural" damage threshold but must have been due to a rather imperfect surface and/or inclusions. Indeed, optical quality alkali halide samples from Harshaw have a large number of inclusions

and also a rather poor surface finish. (Large scratches are easily visible when the surface is illuminated with a microscope lamp.)

This damage occurred at photon flux levels below that required, on the basis of processes described in the previous section, to obtain the observed[1] exoelectron images. Therefore, the exoelectron images observed[1] on LiF surfaces after exposure to intense light from a Nd-glass laser cannot be explained by multiphoton processes assumed in the preceding section. What then is their nature and what is the mechanism responsible for their formation? The answer to this question has important implications concerning the goal of this research effort. We therefore performed a series of experiments which yielded convincing evidence that the occurrence of a spark or plasma is required for the image formation in LiF. This spark is, under certain conditions, not associated with any kind of visible damage. We note that no plasma formation, either in air or on the surface of the sample, is assumed. As a point of interest, this condition of no plasma will best be achieved using a TEM_{00} mode laser up to the threshold power density for air breakdown or for breakdown of the sample surface accompanied by a white-hot plasma. Multi-mode laser beams will in general produce air breakdown or damage of the sample surface at lower power densities (these are necessarily <u>average</u> power densities) due to the well-known occurrence of high power filaments.

In a first set of experiments, we exposed a 1 in. x 1 in. LiF crystal of optical quality to 9 shots of the Owens-Illinois Nd-glass laser. Several of those shots, placed on different parts of the sample, produced damage without the formation of a spark. The occurrence of a spark was monitored with a photographic camera. Damage occurred at 20 J/cm^2 for a 30 ns pulse. None of the sites damaged in the absence of a spark emitted exoelectrons in the familiar "doughnut" pattern;[1] for that matter, no exoelectron emission was observed at all. We continued the exposures of different areas of the sample with various beam energies (as low as 1/6 of the damage threshold). (Care was exercised to avoid laser bleaching of adjacent laser exposed sites.) No damage occurred under these conditions and no exoelectron emission was detected.

Repeating these experiments with the multi-transverse mode Korad K-1 laser at the Bendix Research Laboratories yielded similar results. Some of these results are shown in Figure 6. In Figure 6(b) the lower three damage sites did not spark and emitted no exoelectrons upon heating.

The upper left damage site was produced with a focused beam (f = 14 cm) that produced air breakdown. The sample was placed in the center of the air spark. The upper center spot was obtained with the laser power reduced to the air breakdown threshold. Removing the LiF-crystal about 1 cm away from the lens results in an air breakdown spark just in front of the sample. No damage was produced; however, the familiar exoelectron image is clearly observable [Figure 6(a)]. This latter condition therefore produced the effects described in reference 1, that is, no damage but strong exoelectron emission. Moving the crystal away from the focus toward the lens (so that air breakdown in the absence of the sample would occur behind the sample) produced the damage pattern seen in the lower row of Figure 6(b). No sparks were observed and no exoelectron images could be detected. In order to obtain an exoelectron image on the exit face of the crystal, the formation of a spark is again required.

Producing air breakdown in front of the sample (sample surface parallel to laser focal waist) resulted in a cigar-shaped exoelectron image, which is further convincing proof for the "spark" mechanism (Figure 7).

In summary, we observe:

(a) LiF samples of the quality used in our experiment (Harshaw, optical finish) damage well below their expected dielectric breakdown threshold (calculated from measured dc breakdown data). This is most likely due to the rather poor quality of the sample surface (surface contamination, inclusions, scratches, etc.).

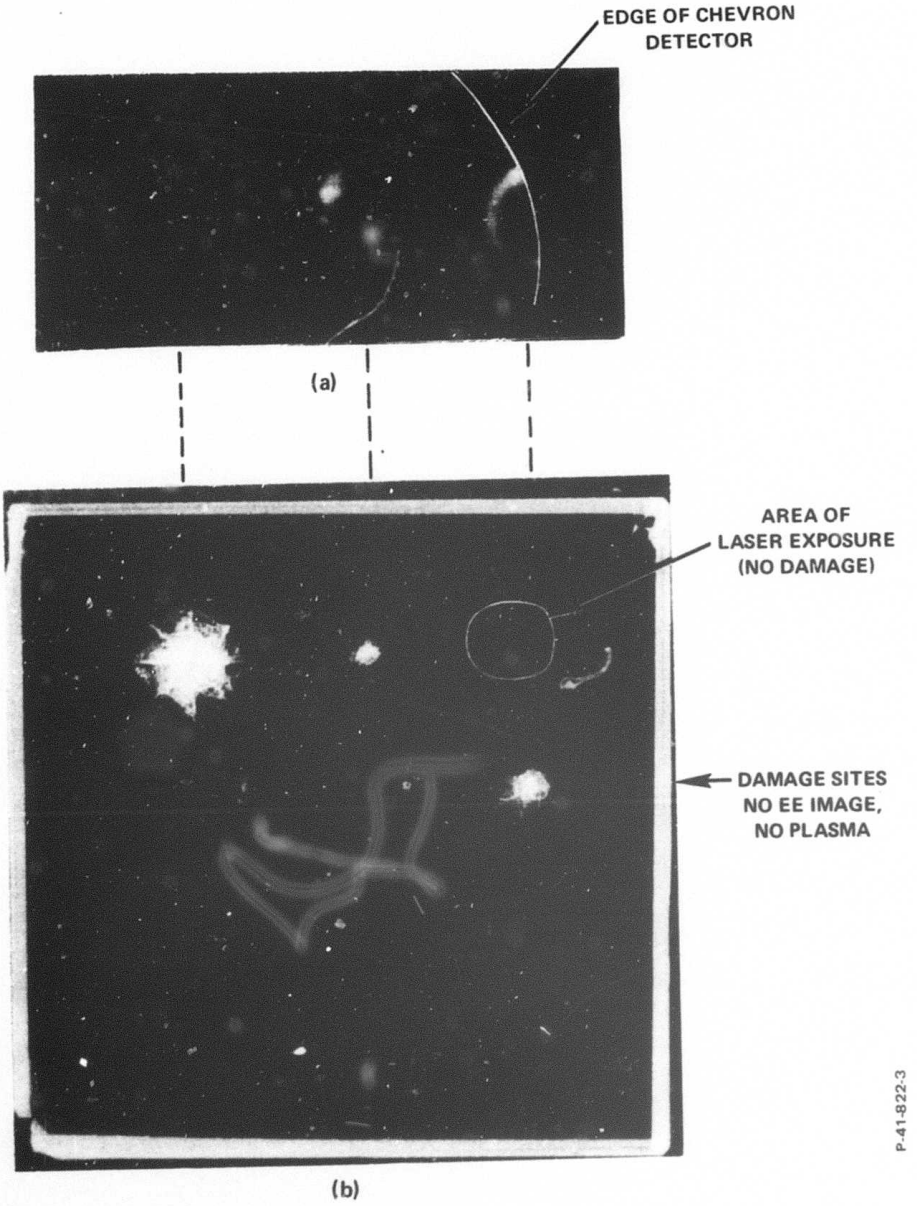

Figure 6 - (a) Exoelectron images on LiF after exposure to intense laser pulses (b) Upper row: areas of laser exposure corresponding to the exoelectron images in Figure 6(a). Lower row: damage sites on LiF that did not produce subsequent exoelectron emission because of the absence of a breakdown plasma during laser exposure.

Figure 7 (a) - Exoelectron image of a LiF single crystal that was placed parallel to the axis of the laser beam waist so that the air breakdown spark occurred in front of the crystal as shown schematically in Figure 7(b).

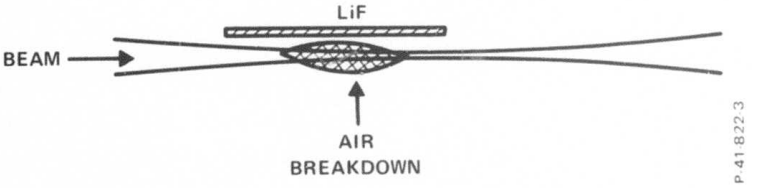

Figure 7(b) - Schematic of the experimental arrangement that resulted in the exoelectron image shown in Figure 7(a).

(b) The formation of an exoelectron image on these LiF surfaces upon exposure to laser photon fluxes $\leq 10^{28}$ cm^{-2} s^{-1} requires the occurrence of a spark (or white-hot plasma), either in air or produced by evaporated sample material, immediately in front of the entrance or exit surface (the surface that the spark occurs in front of is the one that is examined for exoelectron emission).

(c) Under certain conditions (namely, air breakdown a few mm in front of the surface), the familiar exoelectron image can be observed <u>without</u> any visible damage (inspection with magnifying glass). This is the condition described in reference 1 and produced in Figure 3 of this paper (reference 1).

(d) Since the occurrence of sparks is - except under the special circumstances described above - of no interest within the framework of this contract, we will not investigate the processes that lead to exoelectron image formation under this condition.

(e) The computer calculations indicate that an exoelectron image can be formed without sparks. Samples of much better surface quality must be obtained for the experimental investigation of this phenomenon which is expected to occur at photon fluxes $>10^{28}$ cm^{-2} s^{-1}. The influence of the temperature rise during laser exposure and its role in the damage mechanism are questions of interest that we will investigate in the next reporting period.

SECTION 4

EXPERIMENTS ON EXOELECTRON EMISSION FROM SELECTED LASER MATERIALS

In this section we report experimental data on exoelectron emission from ED-2 glass, NaCl, and $LiNbO_3$. Thermally and optically stimulated experiments were conducted.

4.1 THERMALLY STIMULATED EXOELECTRON EMISSION (TSEE)

4.1.1 Apparatus Modifications

An experimental system for the measurement of exoelectron properties of laser materials was described in the preceding semiannual report. Since then, the system has been improved. In particular, the exoelectron gun has been calibrated and its yield improved. Figure 8 shows a schematic of the electron gun. It now operates as expected. Also, signal gain was increased and noise was reduced in the electronics. The detection electronics are shown schematically in Figure 9.

The copper-block sample holder had to be modified to prevent detection of exoelectron emission from the copper. Figure 10 shows TSEE from the holder without a sample crystal after exposure to 3 keV electrons (6×10^{-7} A/cm^2) for 2 min; the erratic behavior of the temperature was due to a loose thermocouple which was subsequently corrected. A peak was observed to occur in the vicinity of the NaCl peak. The holder was then shielded with tantalum foil leaving only the sample crystal exposed to the detector. Tests on tantalum foil (Figure 11) showed that TSEE was negligible. Figure 12 shows TSEE from a tantalum-shielded NaCl crystal.

4.1.2 TSEE from ED-2 Glass

As described in the previous semi-annual report, TSEE was observed from optical quality ED-2 Nd-doped glass samples (Owens-Illinois) after exposure to the Owens-Illinois, high intensity Nd-glass laser (TEM_{00} mode). The emission was very weak and could not be correlated with previous exposure of the sample to the laser light. Since then, we observed

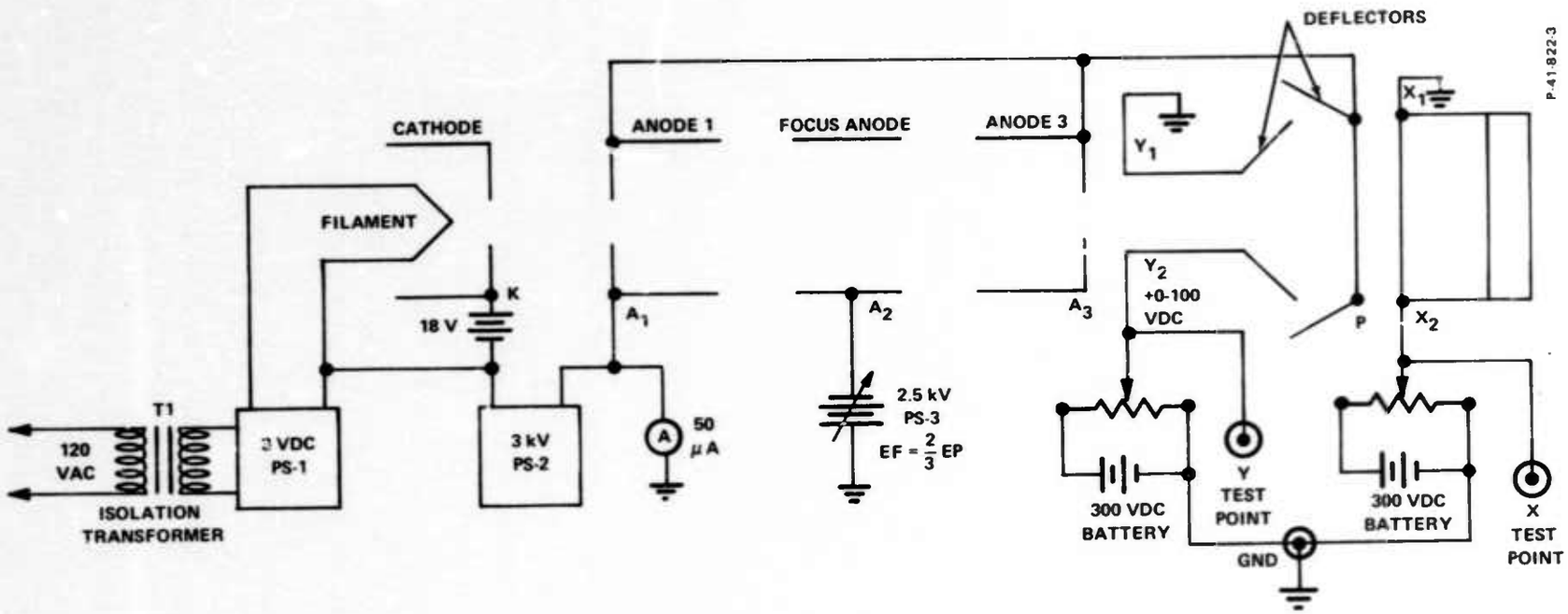

Figure 8 - Electron gun schematic

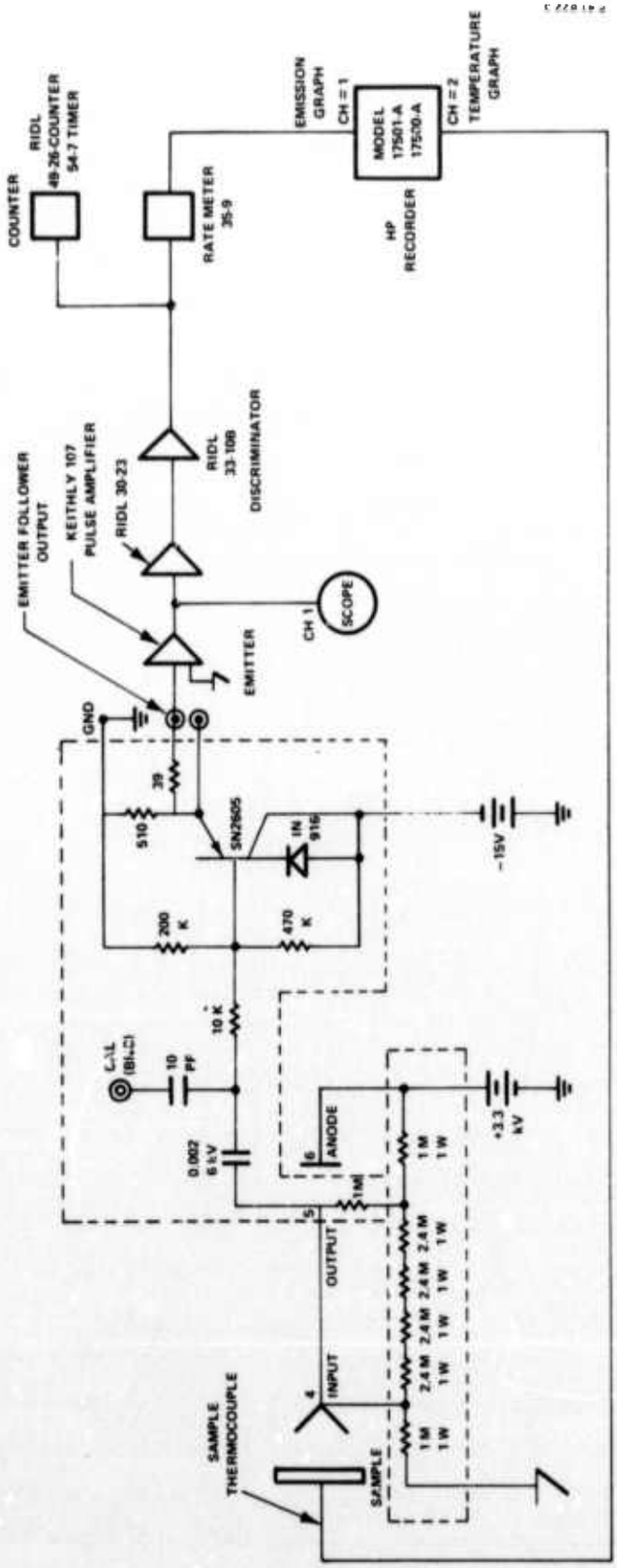

Figure 9 - Detection electronics

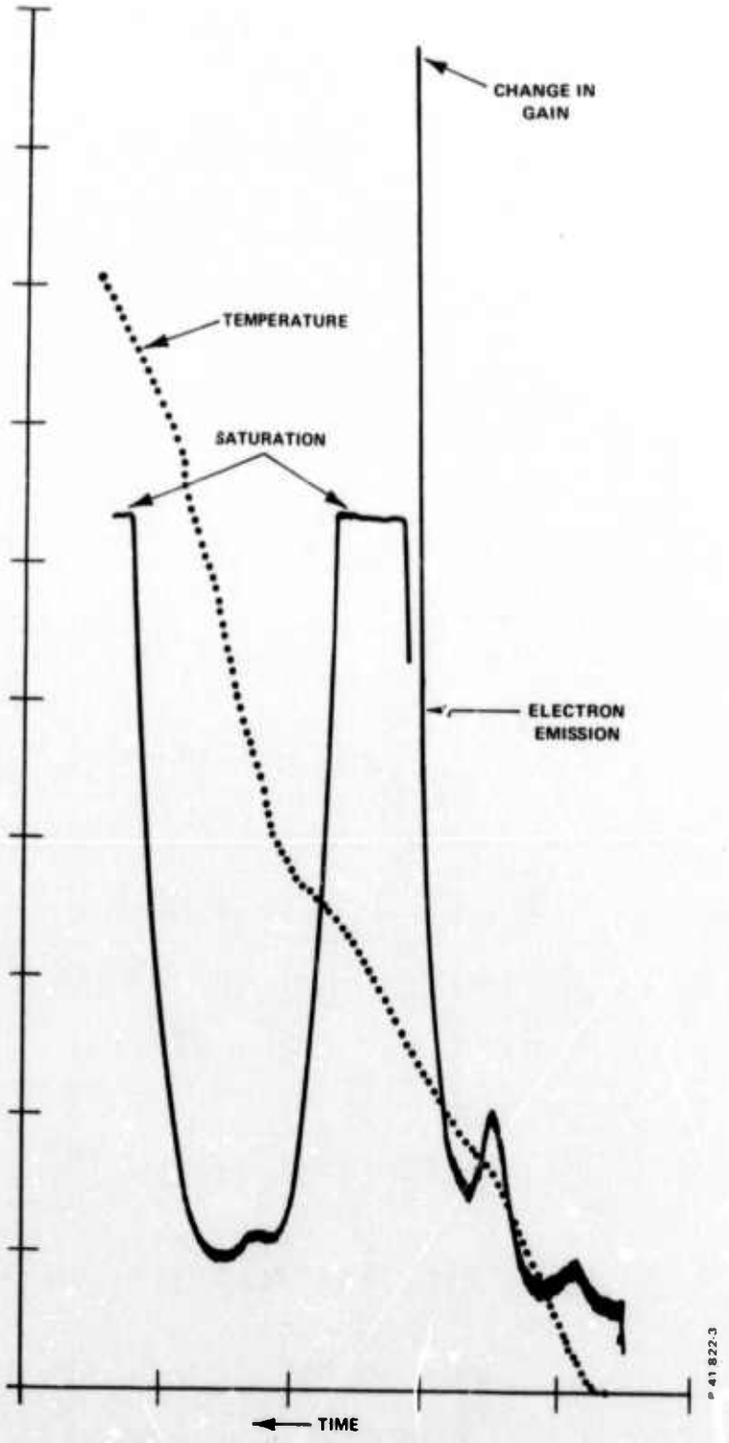

Figure 10 - Electron emission from copper sample holder.

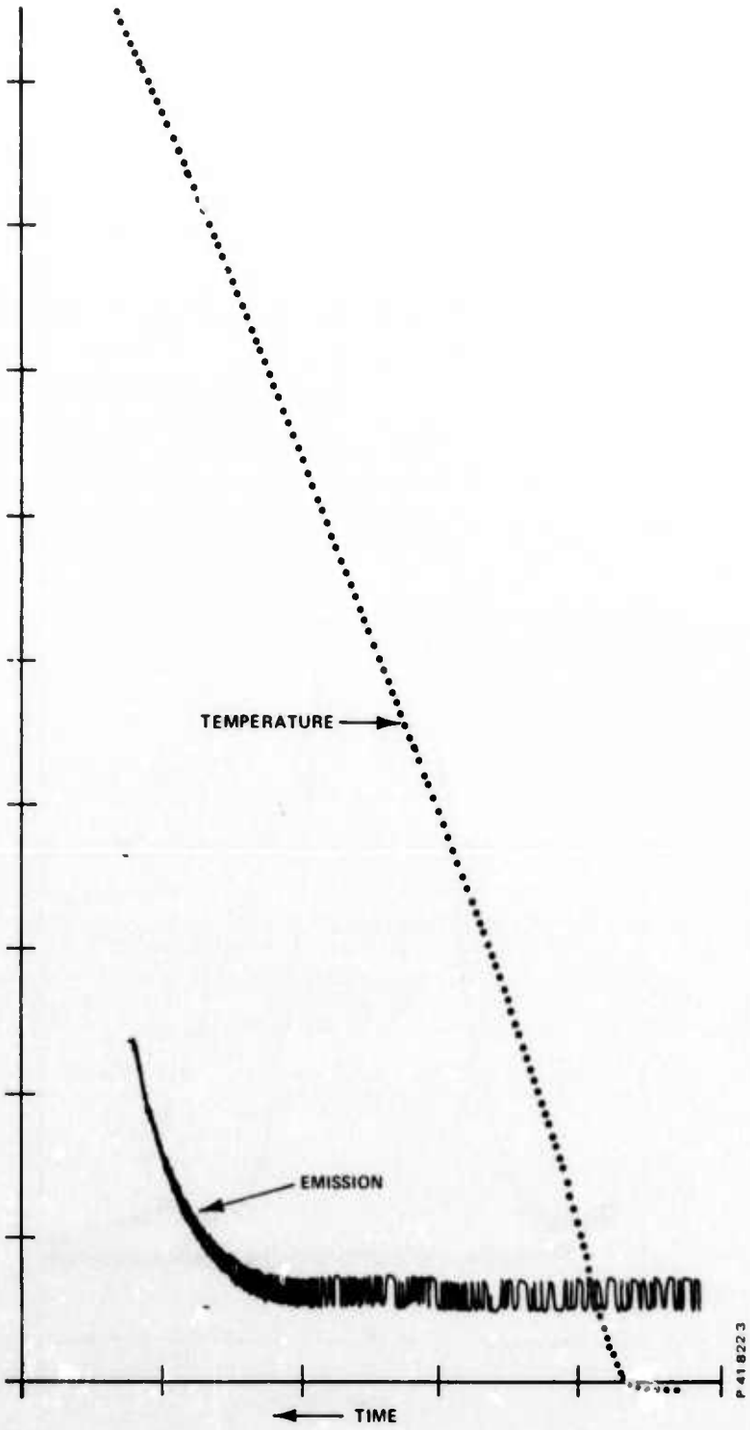

Figure 11 - Electron emission from tantalum.

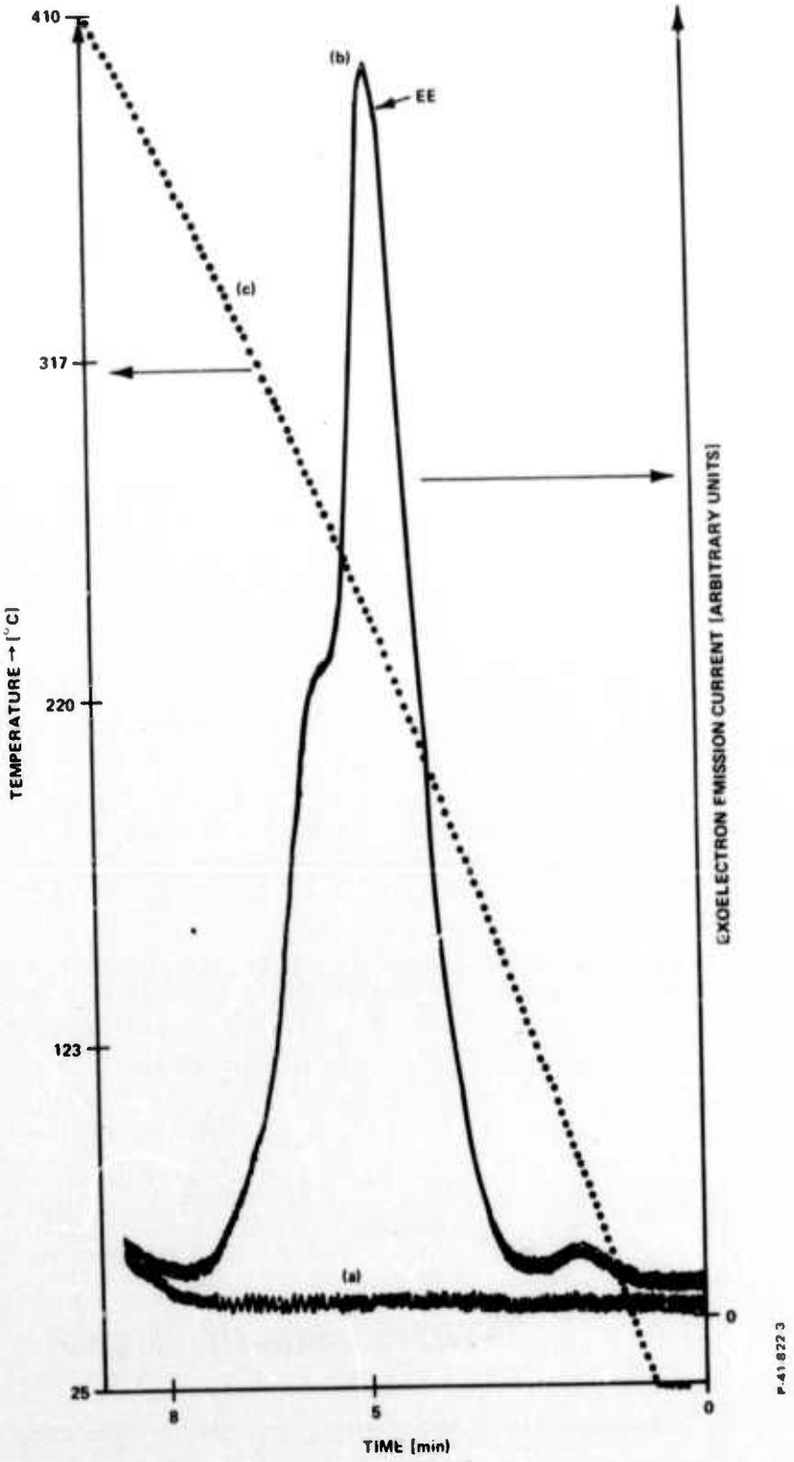

Figure 12 - TSEE from NaCl: (a) exoelectron emission after electron excitation, (b) emission with no prior electron excitation, and (c) temperature profile.

TSEE from ED-2 glass samples after electron bombardment. Typical results are shown in Figure 13. At this point, we have to conclude that the emission is too weak to be of any practical use in laser damage studies.

4.2 OPTICALLY STIMULATED EXOELECTRON EMISSION (OSEE) FROM SINGLE CRYSTAL SURFACES OF $LiNbO_3$ AND NaCl

4.2.1 OSEE from Electron-Irradiated Samples

A newly discovered effect in pyroelectrics was described in the first semi-annual report. We observed strong thermally induced electron emission from a single crystal of $LiNbO_3$ without prior excitation by ionizing radiation. This effect is attributed to thermally stimulated field emission (TSFE). As a result of this effect, the observation of TSEE from pyroelectric materials is difficult if not impossible; TSFE is, in general, a much stronger effect. Optical stimulation has to be used to release trapped electrons.

4.2.1.1 Unpolished $LiNbO_3$ Surfaces

An example of the characteristic decay observed in OSEE is shown in Figure 14 for single crystal, single domain $LiNbO_3$. The surface was ground after the crystal was cut from the boule, but not polished. The c^+ face was first bombarded with unfocused 3 keV electrons. The emission shown as curve "a", which is typical of data* obtained at an early stage of our OSEE investigations, was found to be very reproducible over a span of approximately four runs. By "reproducible", we refer to the peak height and decay rate. A "run" consists of electron bombardment of the surface and subsequent illumination with photons. In these tests, the decay rate and peak height were observed to depend on the light intensity as expected. However, they were found to be independent of the bombarding electron exposure time t_e. Since the peak height and decay rate should also depend on the number of populated electron traps, the observed time independence probably indicates complete population of the

*Unless otherwise indicated, the emission calibration was $\sim 10^5$ counts/min full scale; the bombarding electron current was 6×10^{-7} A/cm^2.

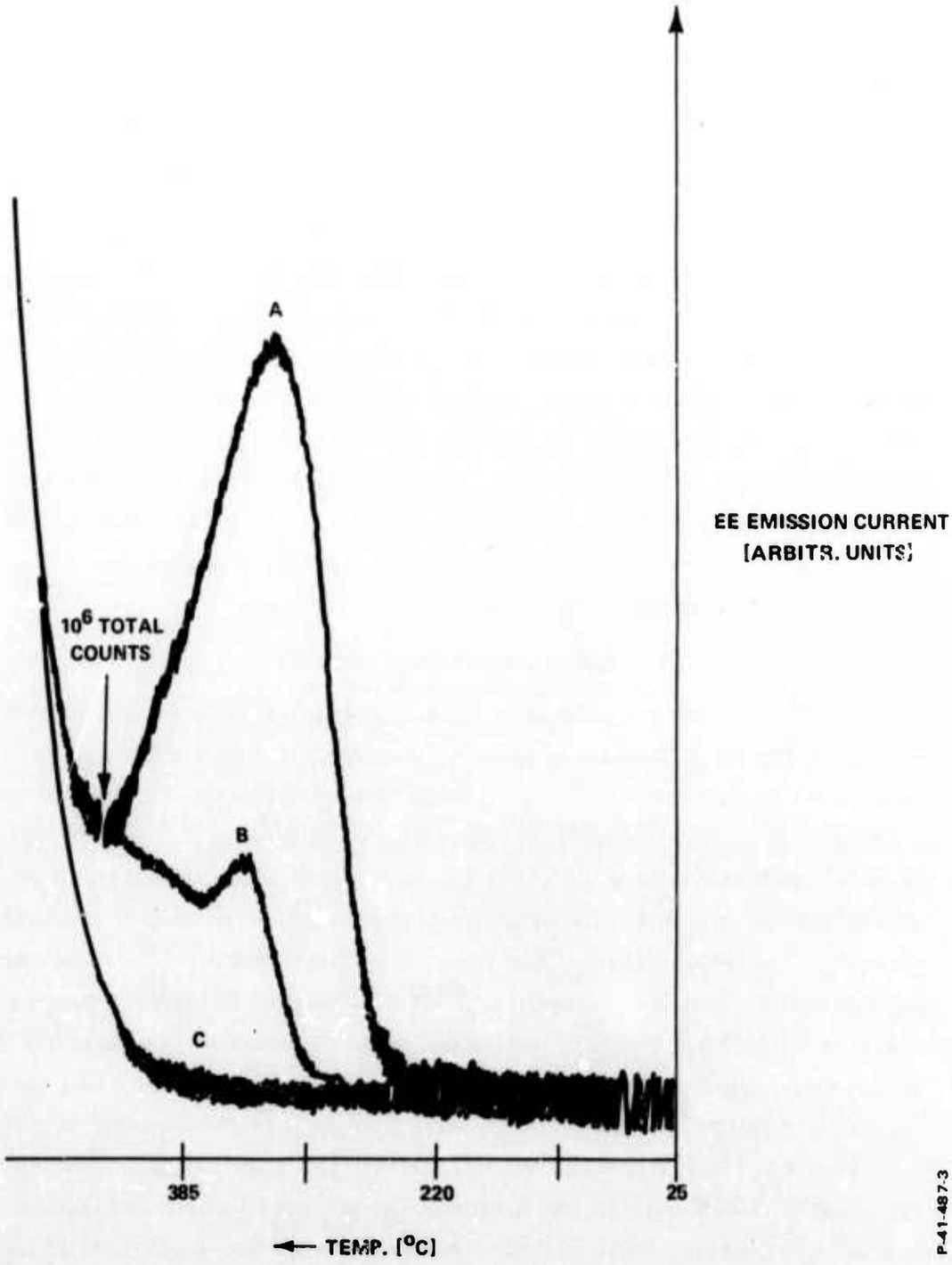

Figure 13 - TSEE from ED-2 glass after electron bombardment (3 keV, 6×10^{-7} A/cm^2) for: (a) 10 min, (b) 150 s, and (c) 0 s.

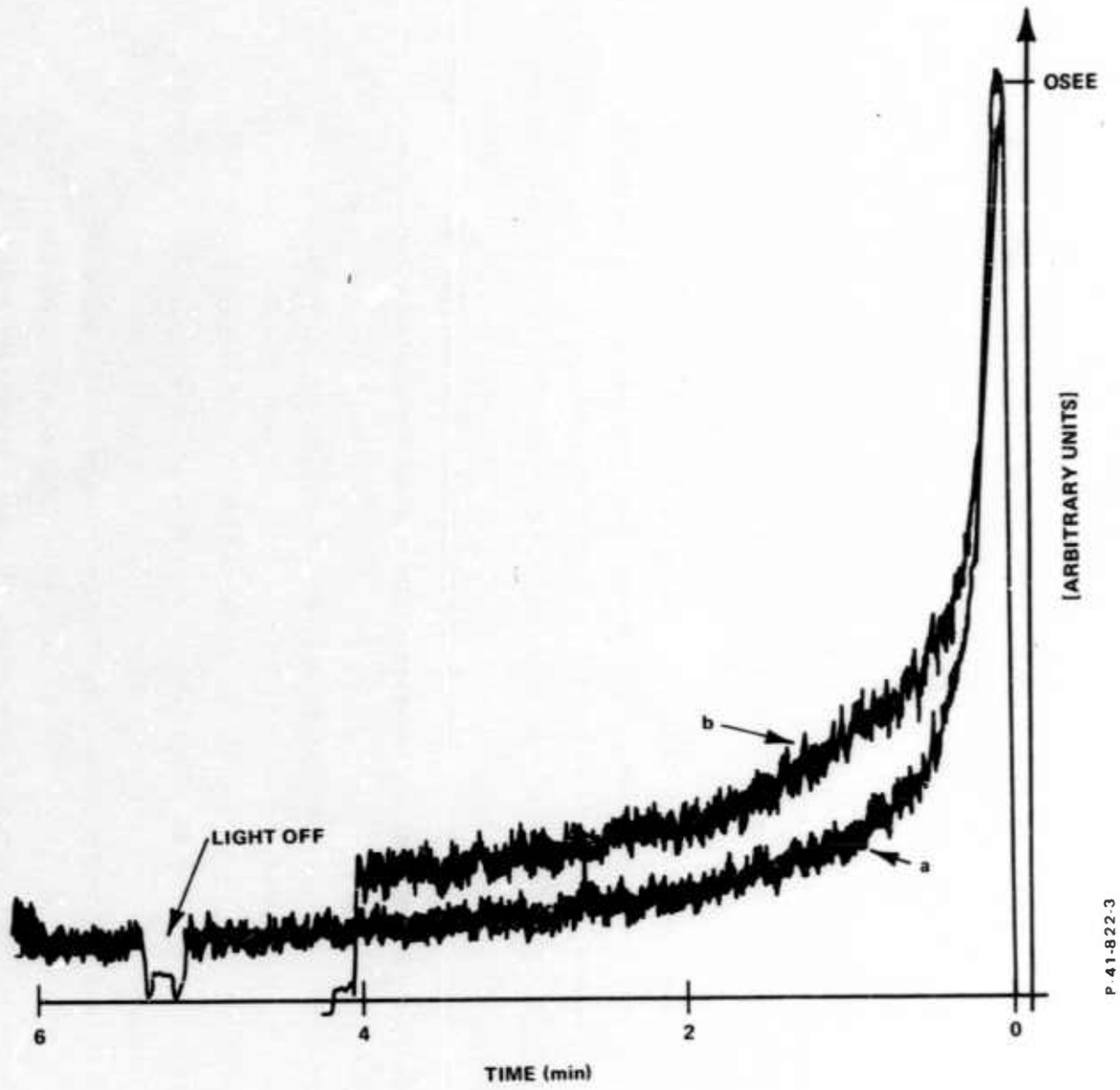

Figure 14 - OSEE from c^+ face of $LiNbO_3$: (a) early run and (b) later run.

pertinent traps. Curve 14b, which was taken under the same operating conditions about 12 runs after 14a, shows a different decay rate. This new rate, which persisted in subsequent runs, is indicative of a change in surface conditions. Most likely, the change was due to the electron bombardment.

There was some indication that several different rates were involved in the decay. This became evident in further tests. In one of these tests, the kinetic energy of the bombarding electrons was varied. Figure 15 shows the variety of emission patterns encountered for energy changes of 1 to 3 keV with t_e ~5 minutes. Results of tests involving the variation of t_e are shown in Figure 16; 2.5 keV electrons were used. The variation in the emission is shown in Figure 17 for fixed operating conditions (t_e ~1.5 min and the kinetic energy of the bombarding electrons was 2.5 keV). The emission was observed to increase fivefold when the accelerating voltage was decreased from +600 to +300 V. Emission was still detected with a retarding voltage of -600 V; it decreased by a factor of ~3.5 when the sample-detector voltage was changed from +600 to -600 V.

A very curious effect was observed when a time delay (t_d) was introduced between the end of the electron bombardment period and the start of the photon illumination period. Figure 18 shows emission results obtained from a series of runs in which different t_e and t_d were used. A second emission peak appears somewhat "spontaneously" approximately 0.5 to 0.75 min after the decay of the first peak. The interval between the two peaks increases with t_d and t_e. For comparison, an emission curve for zero delay (i.e., $t_d = 0$) is also shown in Figure 18; this run was performed during the same series as the other three.

In an effort to determine whether the crystal orientation affected the emission, we also conducted a series of experiments on the c^- face. Figures 19(a) and (b) show OSEE after a 3-min exposure of the c^- face of the $LiNbO_3$ crystal to 2.5 keV electrons. These curves are typical of the variation in the emission pattern encountered for fixed operating conditions. The curve shown in Figure 19(b) was obtained from the run immediately following the run which produced

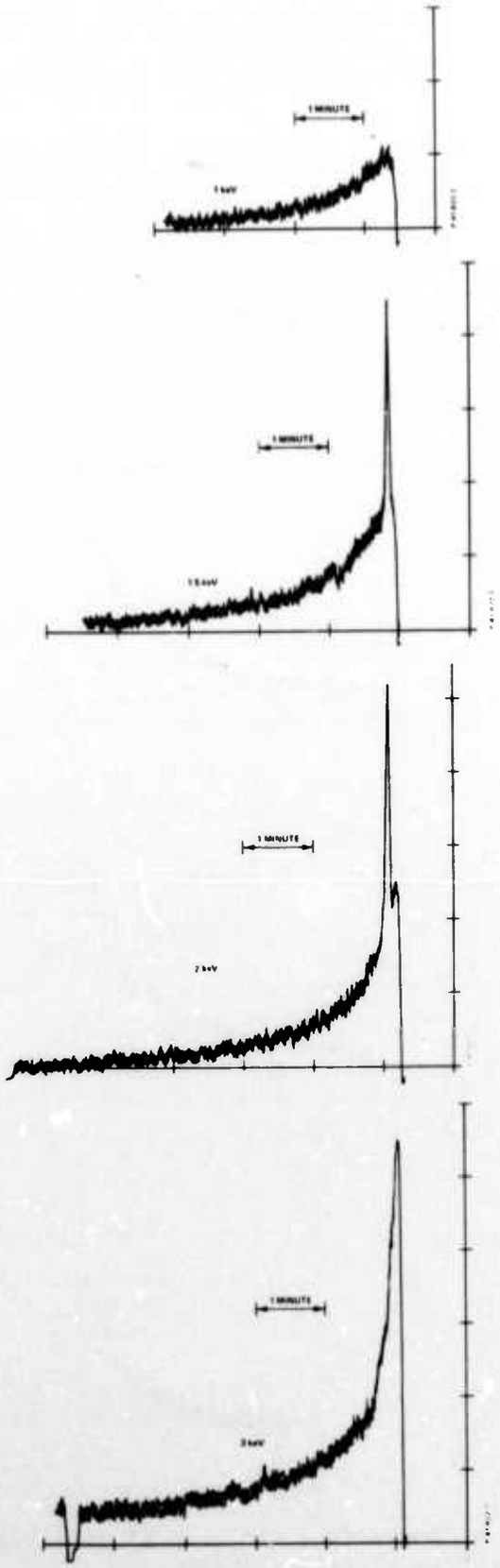

Figure 15 - Effect of kinetic energy of bombarding electrons (5 min exposure) on OSEE from c^+ surface of $LiNbO_3$.

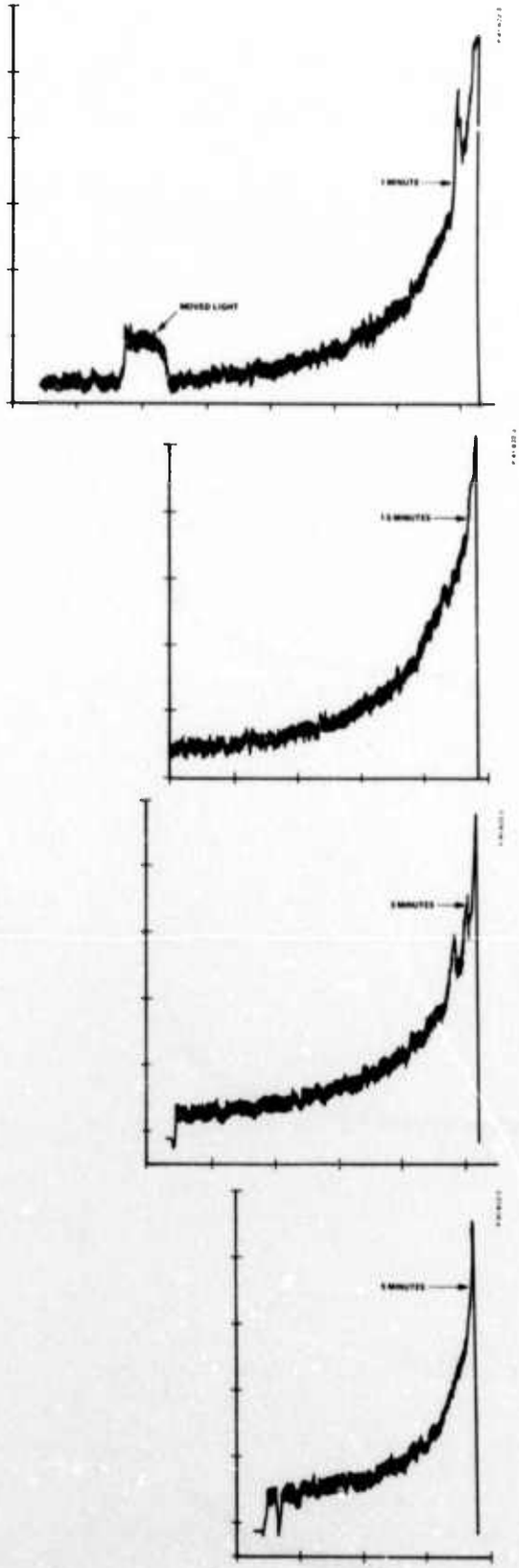

Figure 16 - Effect of bombarding electron (3 keV) exposure time on OSEE from c^+ face of $LiNbO_3$.

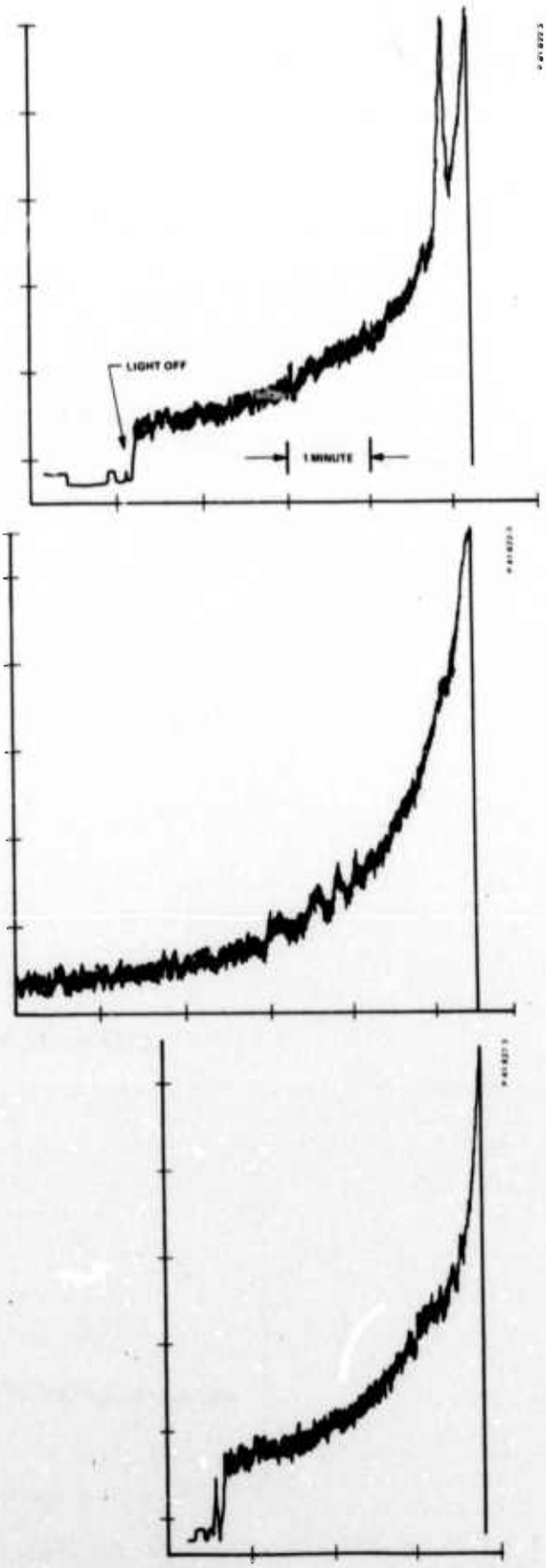

Figure 17 - Typical variations in OSEE from c^+ face of $LiNbO_3$ for fixed operating conditions.

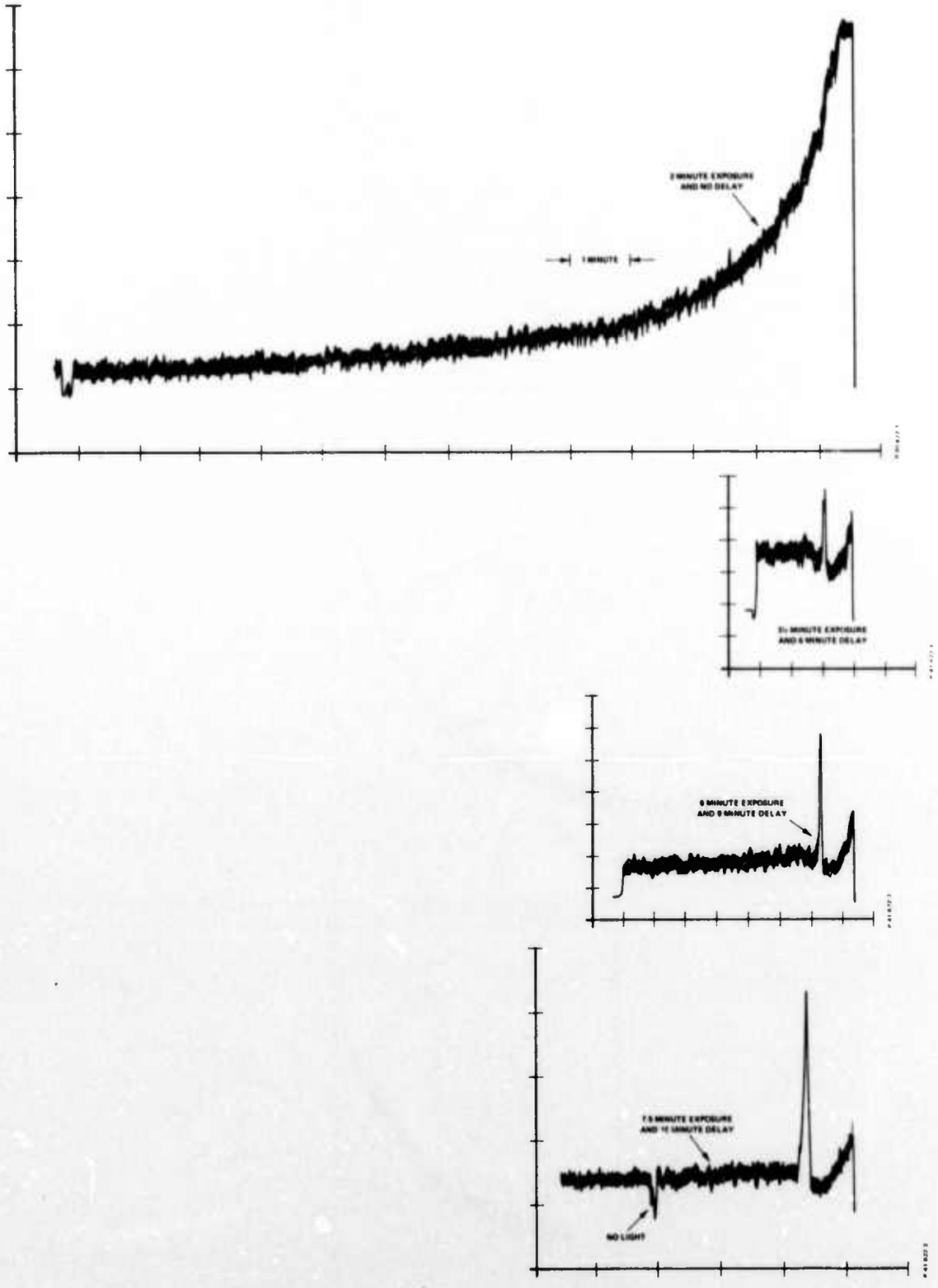

Figure 18 - Effect of delay and exposure time on OSEE from c^+ face of $LiNbO_3$.

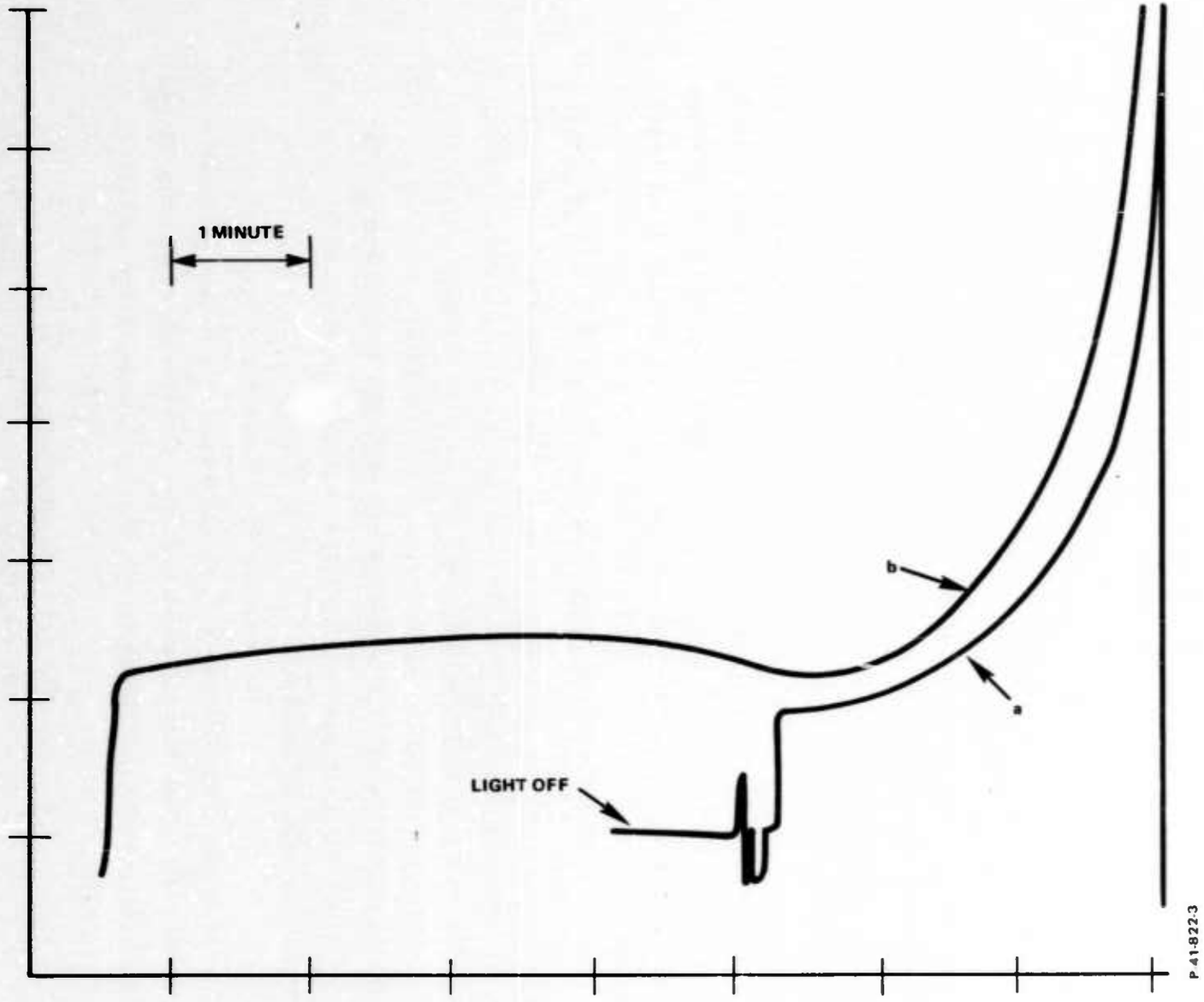

Figure 19 - OSEE from c^- face of $LiNbO_3$ ($t_d = 0$). Run "b" was taken immediately after "a".

Figure 19(a). There was no delay (i.e., $t_d = 0$) in these runs. Of particular interest is the small, broad peak observed several minutes after the initial decay. This broad peak was also observed in subsequent runs.

Figure 20 shows several runs on the c^- face in which t_d was varied. Again considerable peak structure is evident. In another experiment, an 11-min delay was introduced after exposure of the c^- face to 2.5 keV electrons for 3 min; Figure 21 shows the resulting emission. Two broad peaks were observed after the initial peak. After these peaks, the light was interrupted for $\sim$0.5 min. As seen in Figure 21, the emission slowly increases after the light is reintroduced, levels off, and then slowly decreases. This light interruption was repeated several times (see Figure 21). The interruption was achieved using a light stop rather than turning the lamp off; the latter would have involved a warm-up period. Just moving the light beam, which illuminates $\sim$75% of the sample surface, around the surface produced similar broad peaking.

Figure 22 shows the effect of a retarding voltage on the emission. The curve in Figure 22(a) shows the emission with an accelerating potential of +300 V applied across the sample detector gap; the effect of interrupting the light is also shown. Figure 22(b) shows the emission with a -3300 V retarding potential. Emission is still observable. It is not clear whether the emission is high energy electrons or ultraviolet light. The latter can also be detected by the channel electron multiplier.

The emission was observed to change from the sharp risetime seen, for example, in Figure 22 to the slow risetime shown in Figure 23. This change, which occurred in the span of one run to the next, could not be attributed to any obvious change in the operating conditions.

4.2.1.2 OSEE from Polished NaCl Surfaces

OSEE from single crystal NaCl is shown in Figure 24 for a 1-min exposure to 2.5 keV electrons. The emission was

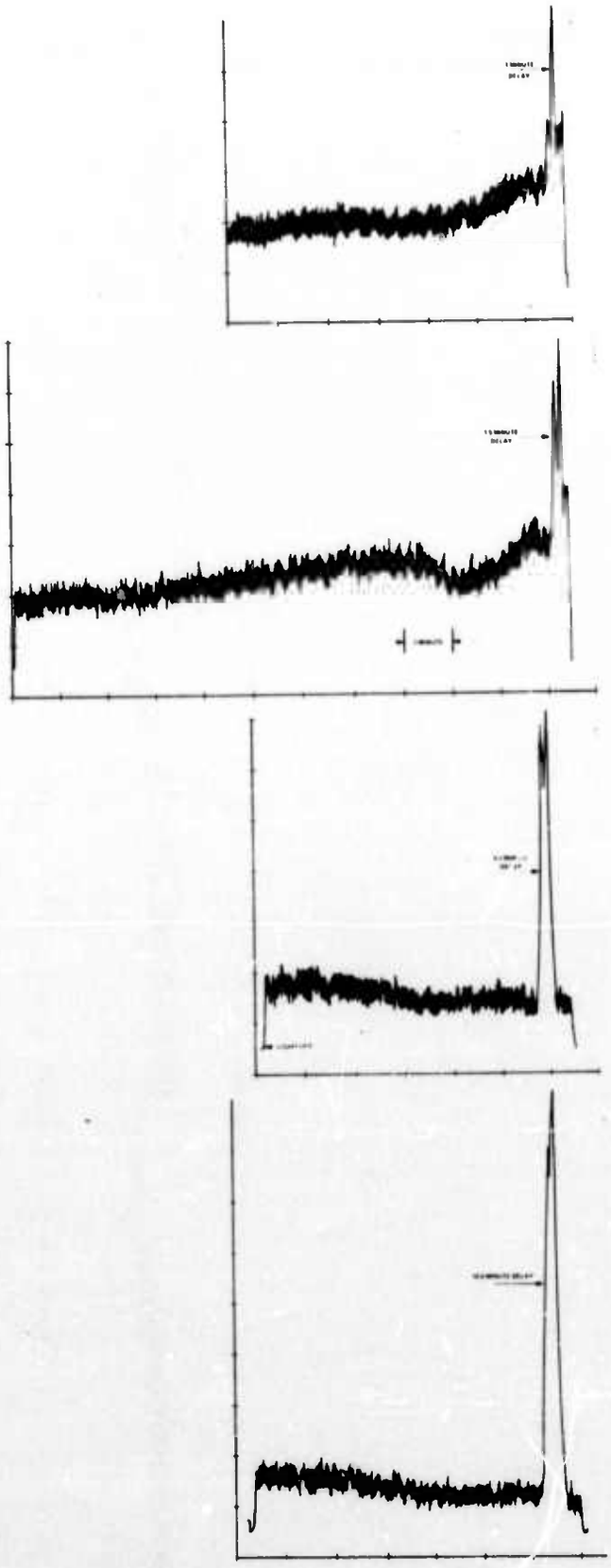

Figure 20 - Effect of delay on OSEE from c^- face of $LiNbO_3$.

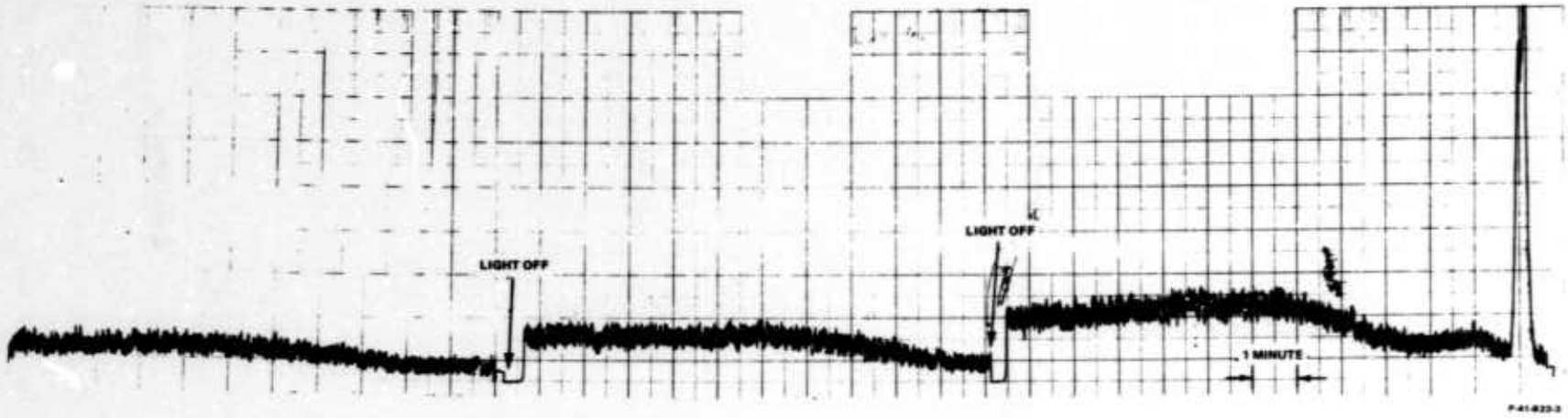

Figure 21 - Effect of light interruptions on OSEE from c^- face of $LiNbO_3$.

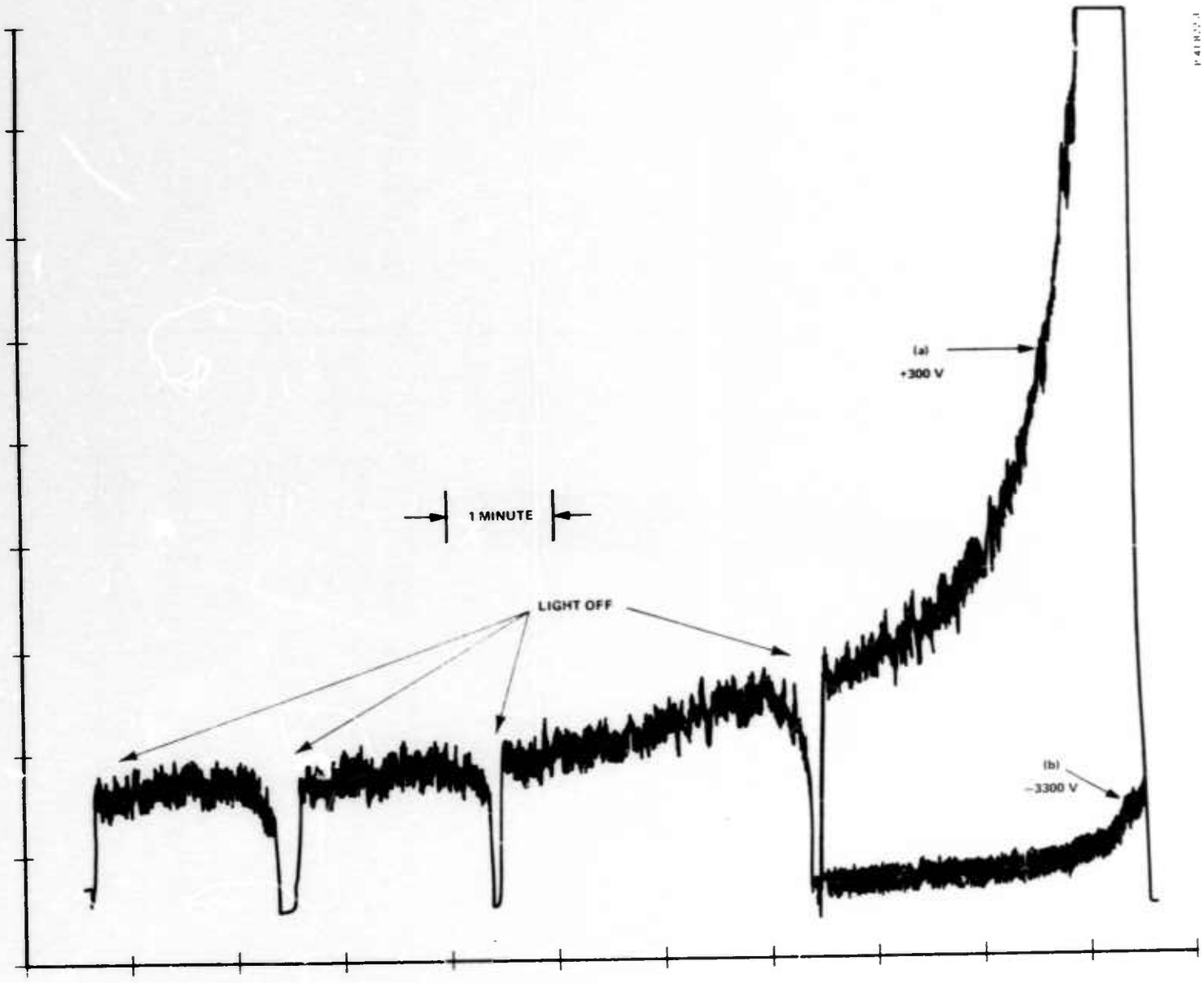

Figure 22 - Effect of retarding voltage on OSEE from c^- face of $LiNbO_3$: (a) accelerating voltage of +300 V and (b) retarding voltage of -3300 V.

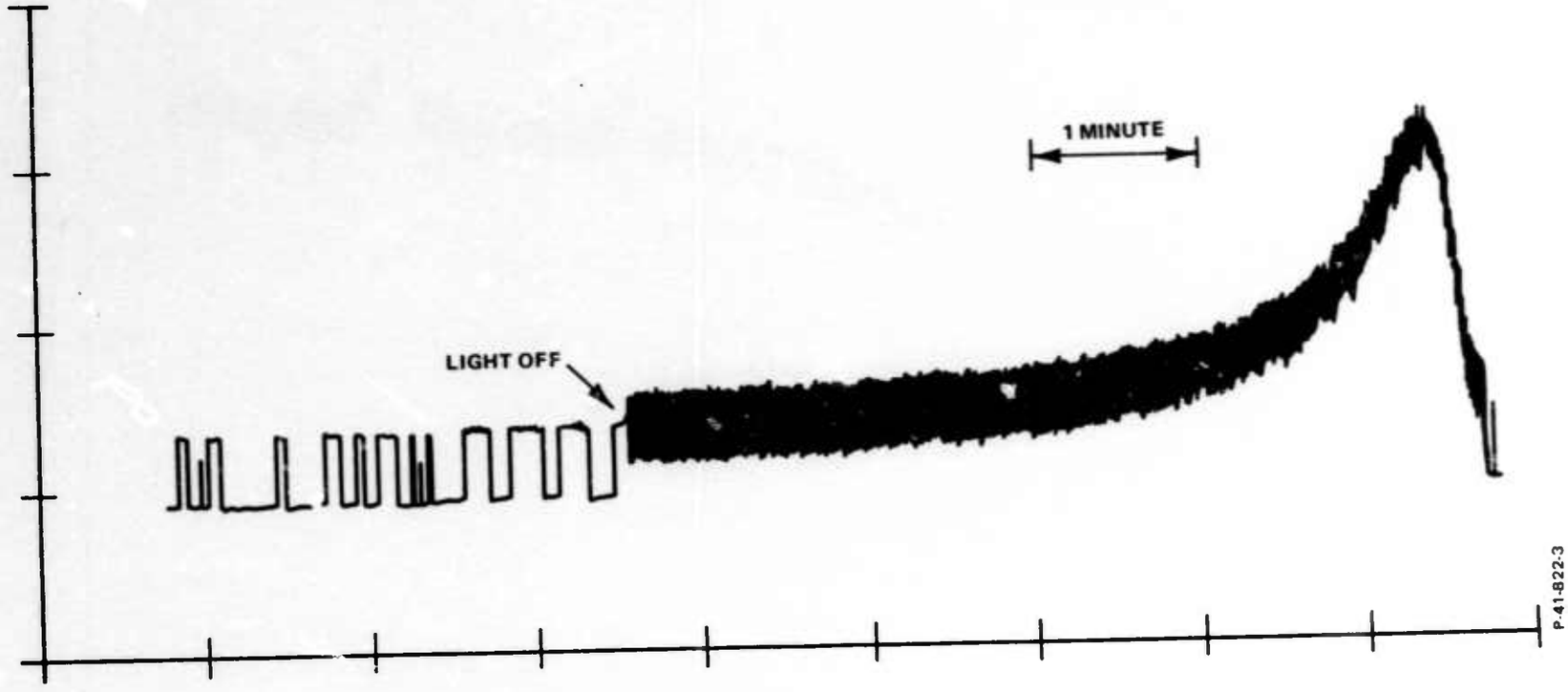

Figure 23 - OSEE from c^- face of $LiNbO_3$ showing risetime changes

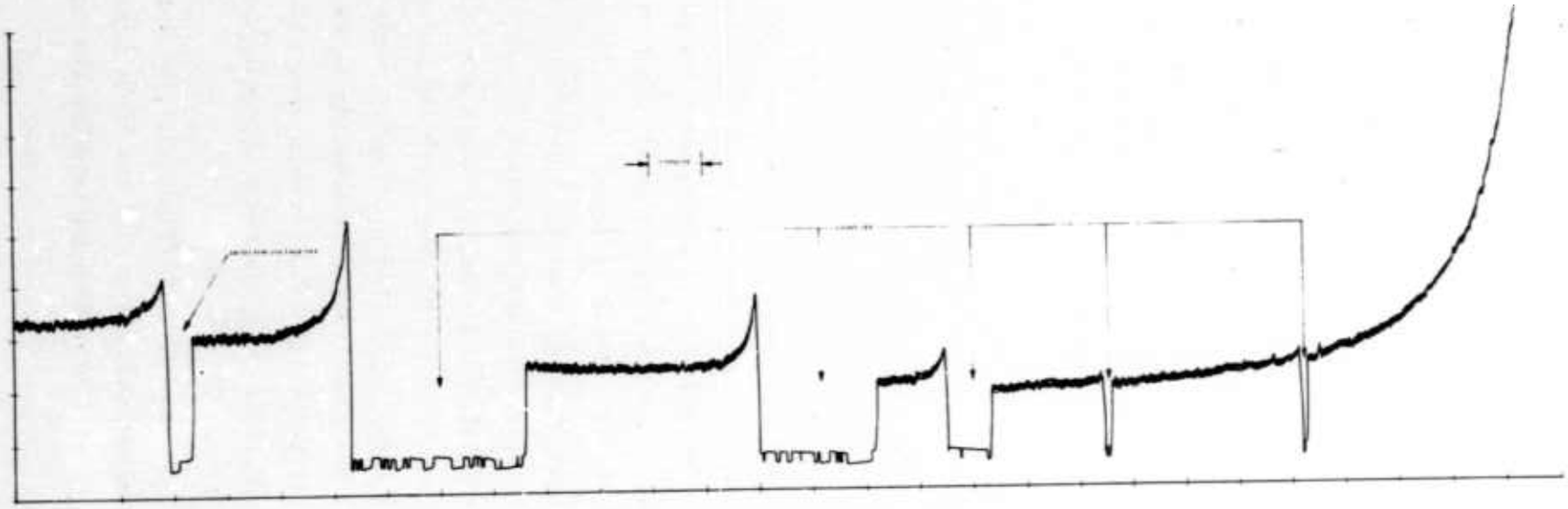

Figure 24 - OSEE from NaCl.

found to be roughly an order of magnitude large than that from $LiNbO_3$ ($> 10^6$ counts/min full scale). Also shown in Figure 24 is the effect of interrupting the light beam and the detector voltage. The peaking which occurred after the interruption is probably due to detector gain fatigue. The sharp rise after reintroducing the light, the high count rate, and the peaking after the voltage interruption all point to this possibility.

4.2.1.3 OSEE from Polished $LiNbO_3$ Surfaces

After the $LiNbO_3$ experiments described in Section 4.2.1.1 were completed, the surfaces of the $LiNbO_3$ samples were diamond-polished; a great deal of care was exercised to avoid altering the crystal orientation. The intent was to identify the effect of the surface finish on the emission. Figure 25 shows a series of OSEE curves for various values of t_e where $t_d < 30$ s. The runs were taken in chronological order beginning with (a) and ending with (d). Two OSEE curves for different values of t_d are shown in Figure 26; curve (b) was taken after (a). After two days of no experimentation, the curve shown in Figure 27 was taken.

The emission in subsequent runs was observed to be about an order of magnitude lower than that obtained in Figures 26 and 27. This change could not be related to any obvious change in the operating conditions. We therefore suspect that the surface conditions were changing. Because of this possibility, an effort to correlate the data of the preceding figures with the t_e and t_d changes was not warranted. We therefore undertook a new series of runs which are shown in Figures 28 and 29; the curves were taken in chronological order beginning with (a). The curves of Figure 29 are particularly interesting since the operating conditions were nominally constant. These curves show that the widths of the "second" peaks and their delay increase chronologically. This was also observed for Figures 25, 26, and 28.

In another test (Figure 30), we introduced various optical filters (red, yellow, and blue) into the light beam. It appeared that the blue filter was least effective in reducing the emission. This

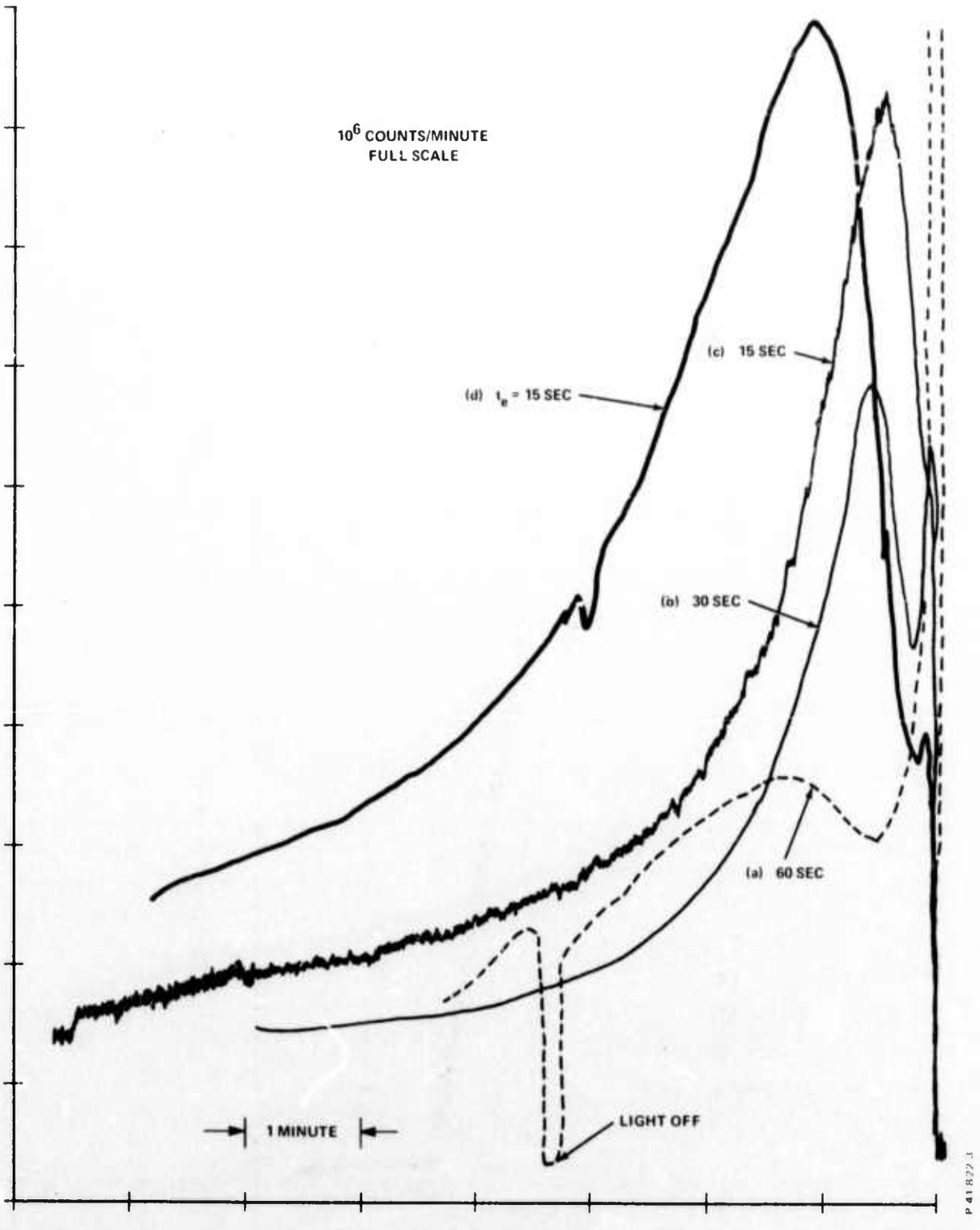

Figure 25 - OSEE from polished $LiNbO_3$ c^+ surface for various t_e ($t_d \lesssim 30$ s)

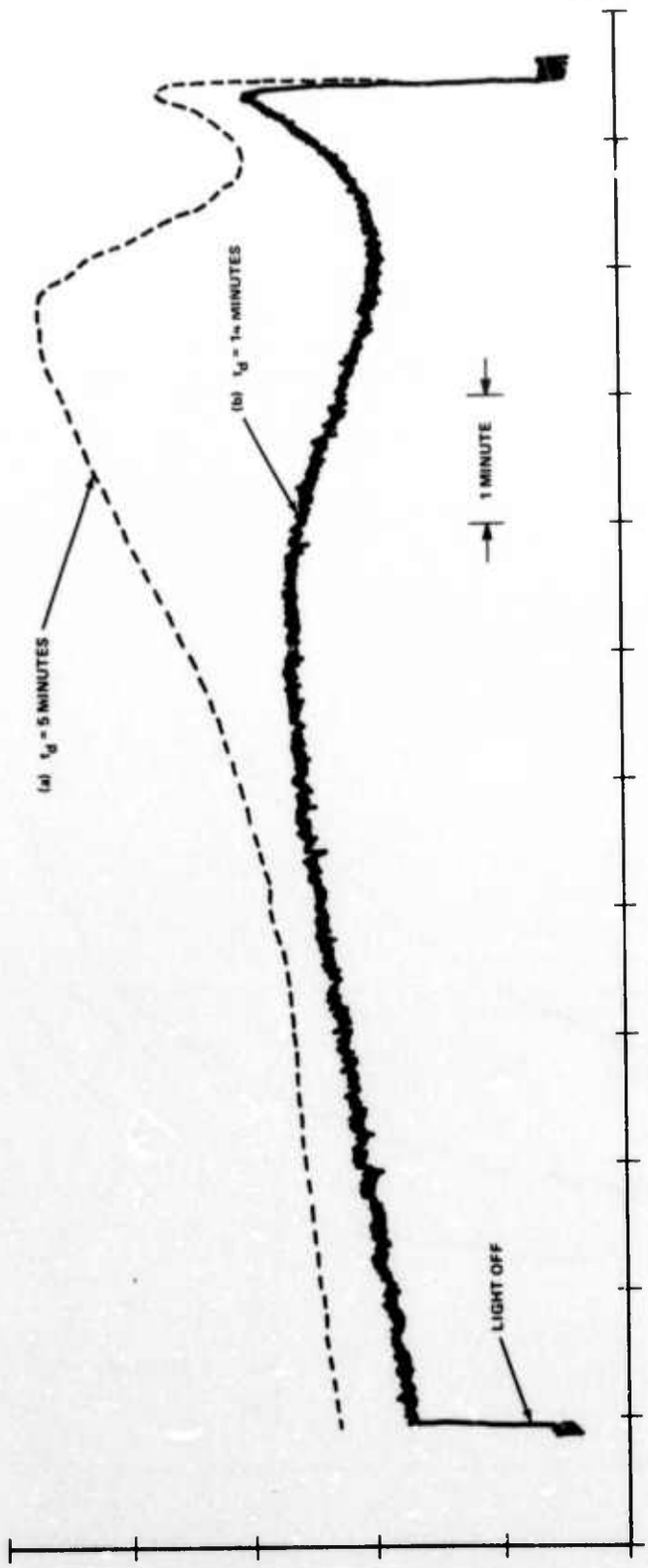

Figure 26 - OSEE curves for different t_d (t_e = 15 s)

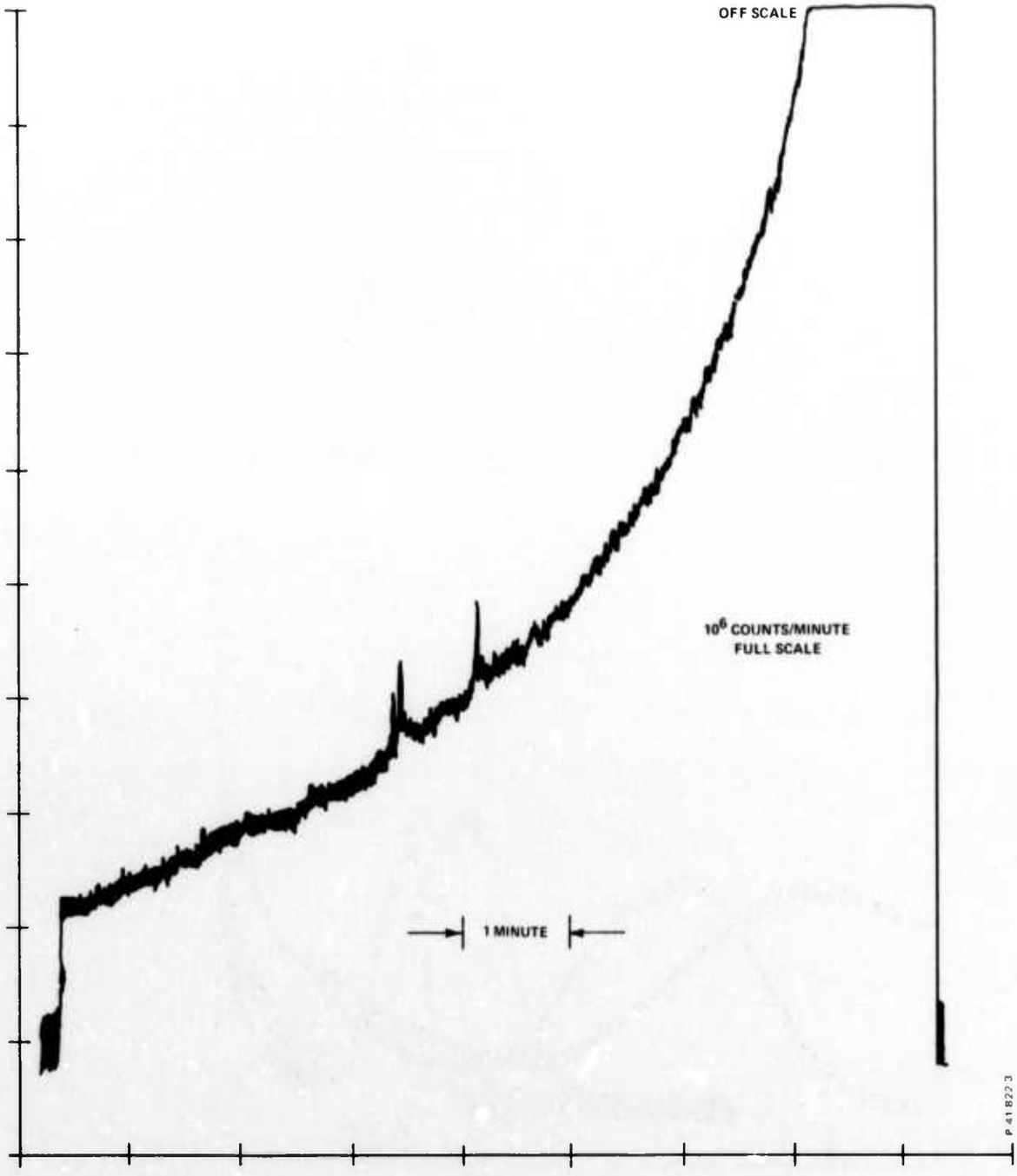

Figure 27 - OSEE for t_e = 5 s.

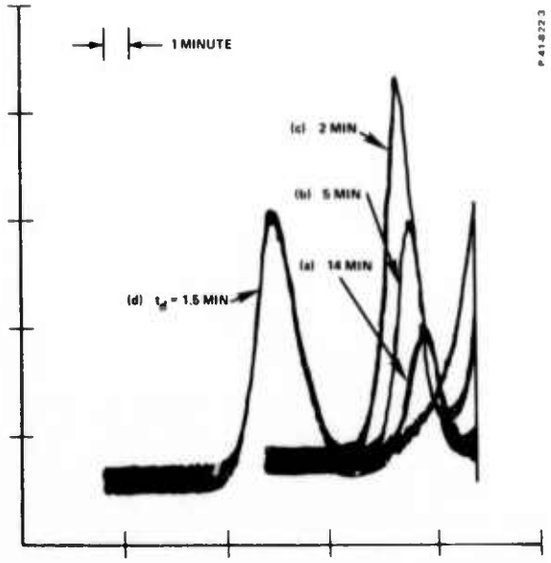

Figure 28 - OSEE for different t_d after decrease in emission

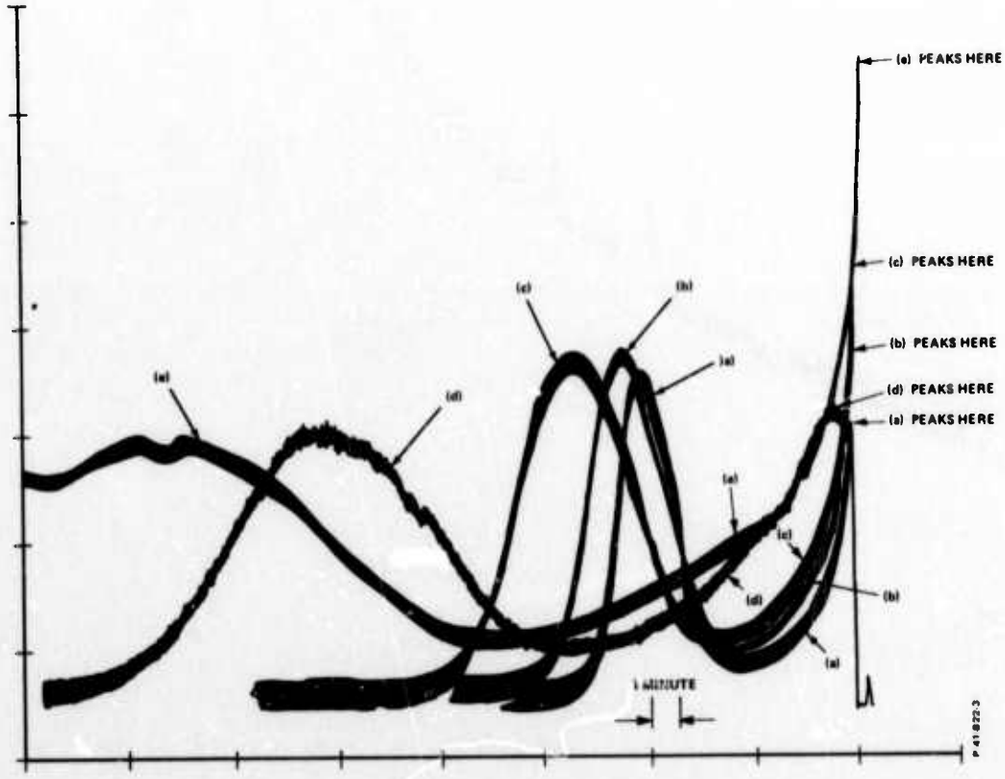

Figure 29 - OSEE after decreased emission for t_e = 15 s and $t_d \leq 60$ s. These runs were taken in chronological order starting with (a) and finishing with (e).

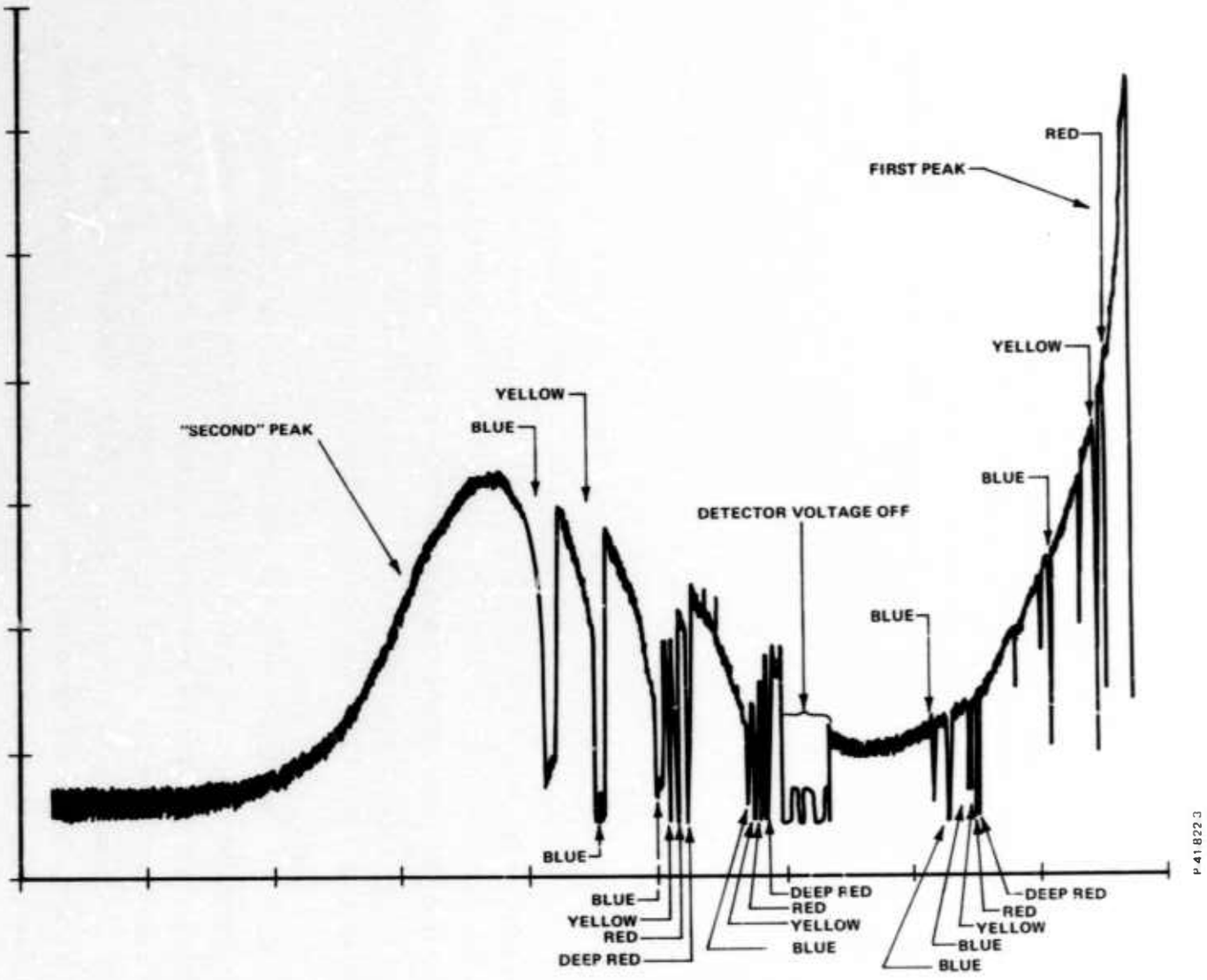

Figure 30 - Effect of wavelength on OSEE (t_e = 15 s and t_d < 30 s)

suggests that the shorter wavelength region of the tungsten lamp was producing the OSEE. Another observation involving the filters is also shown in Figure 30. The risetime after withdrawing the filter is seen to be much slower for the "second" peak. This is possibly indicative of different mechanisms for each peak. In support of this is the observation that the filters appear to extinguish the OSEE associated with the "second" peak more than that associated with the first.

In further runs, the emission decreased to a point where it became difficult to measure. Again, there were no obvious changes in the operating conditions.

4.2.2 OSEE from Laser-Irradiated $LiNbO_3$

Figure 31 shows a schematic of the apparatus employed in our investigations of OSEE from laser-irradiated $LiNbO_3$ crystals. The Q-switched Nd-glass rod laser and the associated monitoring devices were described in the first semi-annual report. In the present work, the laser beam is focused with a 20-cm focal length lens onto the $LiNbO_3$ crystal. Single-domain crystals were used and the surfaces were diamond-polished. The vacuum and detection systems are the same as used in the previously described electron bombardment work. The sample holder was modified, however, to allow the laser beam to pass through the sample and holder. The laser beam was incident on the c^+ side and the detector viewed this side. The tungsten lamp beam irradiated the sample on the c^- side.

An experimental run consisted of exposing the sample to a single laser pulse and then illuminating with the tungsten lamp. The detector and electronics were usually operational during the laser pulse, thereby permitting the signal produced by the interaction of the laser with the sample to be recorded. Since the electronics were very slow ($\gtrsim$100 ms), the resulting signal was, of course, highly integrated. Also, during a run, the beam from the tungsten lamp was usually stopped so that the sample was not illuminated during the laser pulse. In most of the experiments, neutral density filters were used to attenuate the laser beam. The sample was always under vacuum when exposed to the laser pulse.

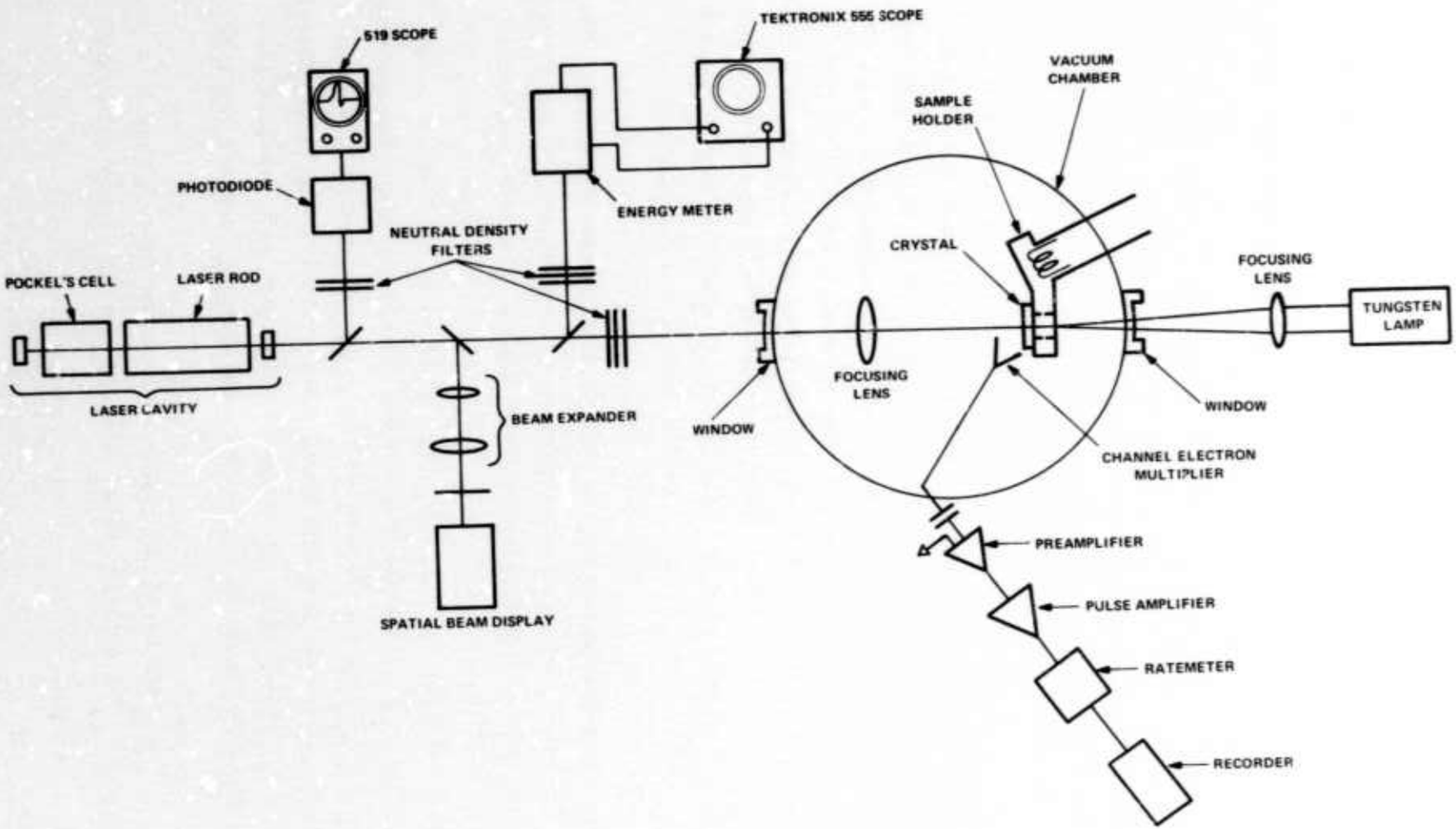

Figure 31 - Schematic of apparatus used in studies of OSEE from laser-irradiated samples

Figure 32 shows the results of several runs taken on a single-domain $LiNbO_3$ crystal which had been exposed previously to ~20 laser pulses ranging in power density from that sufficient to produce surface damage to about 10% of damage threshold. As can be seen in Figure 32, a small emission background resulted when the sample was irradiated with the tungsten lamp ("light on"). During the laser shots, the sample was observed to luminesce with a pinkish color. The four laser shots were taken with the laser beam sufficiently attenuated by neutral density filters to avoid damage to the sample.

Figure 33 shows a series of runs which started with a highly attenuated laser pulse (#1, #2, and #3) and ended with a laser pulse sufficient for surface damage (#5 through #9). We observed the light emission from the sample during the laser exposures in order to determine whether damage occurred. Damage usually occurred when this light was a sharp, dark blue spark. We were not sure whether this spark occurred during the #5 shot. However, it definitely did occur during the #6 shot. We note that the signals for the sixth and subsequent shots begin to exhibit a tail. Also, for the same filter attenuation, the laser signal increased significantly while the OSEE increased only slightly. The OSEE finally became pronounced with the ninth shot. The tail of the laser signal for this shot was quite obvious. Visual inspection of the sample showed slight surface damage. The sample was then exposed at the damaged spot to a series of highly attenuated laser pulses to determine whether the traps (if any) would be excited by low power pulses. Very little emission was observed during the first three shots immediately following the #9 shot of Figure 33; the results are shown in Figure 34. However, the next shot, which was still highly attenuated, produced the emission shown in Figure 35. The next shot produced the emission shown in Figure 36 (#1). The decay time was shorter for this emission.

We then moved the sample so that the laser struck at a different spot. The emission shown after #2 shot in Figure 36 may have

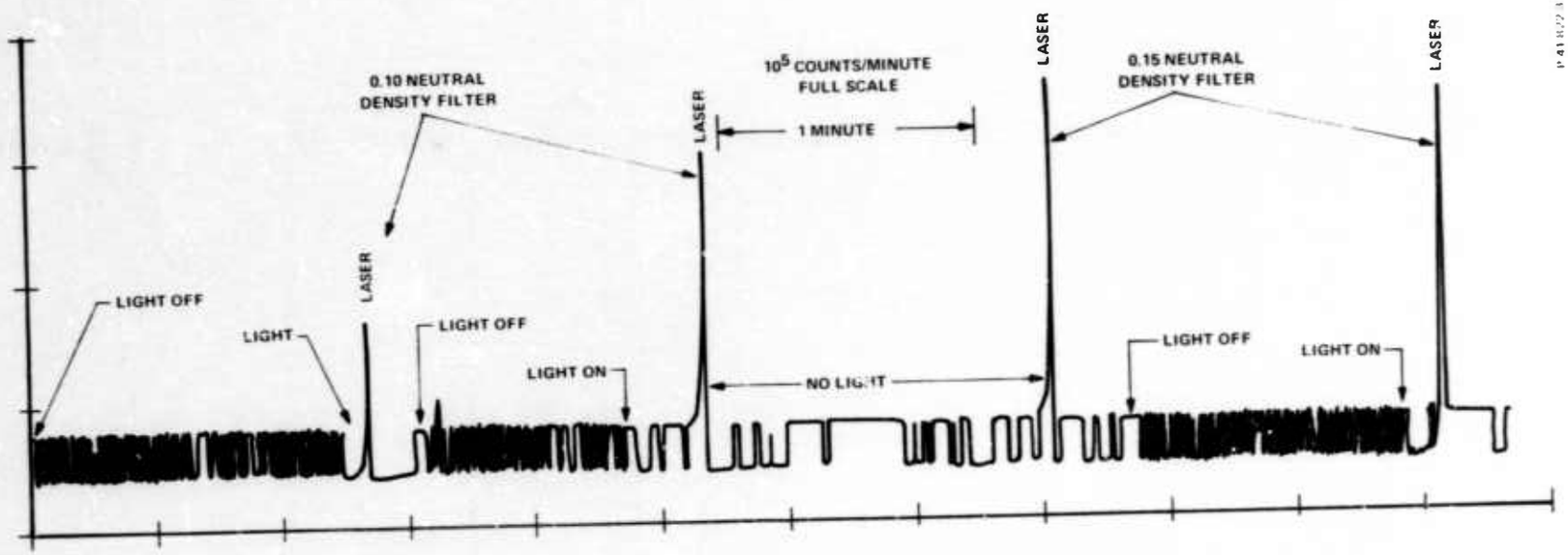

Figure 32 - OSEE from polished c^+ face of $LiNbO_3$ after exposure to weak laser pulses

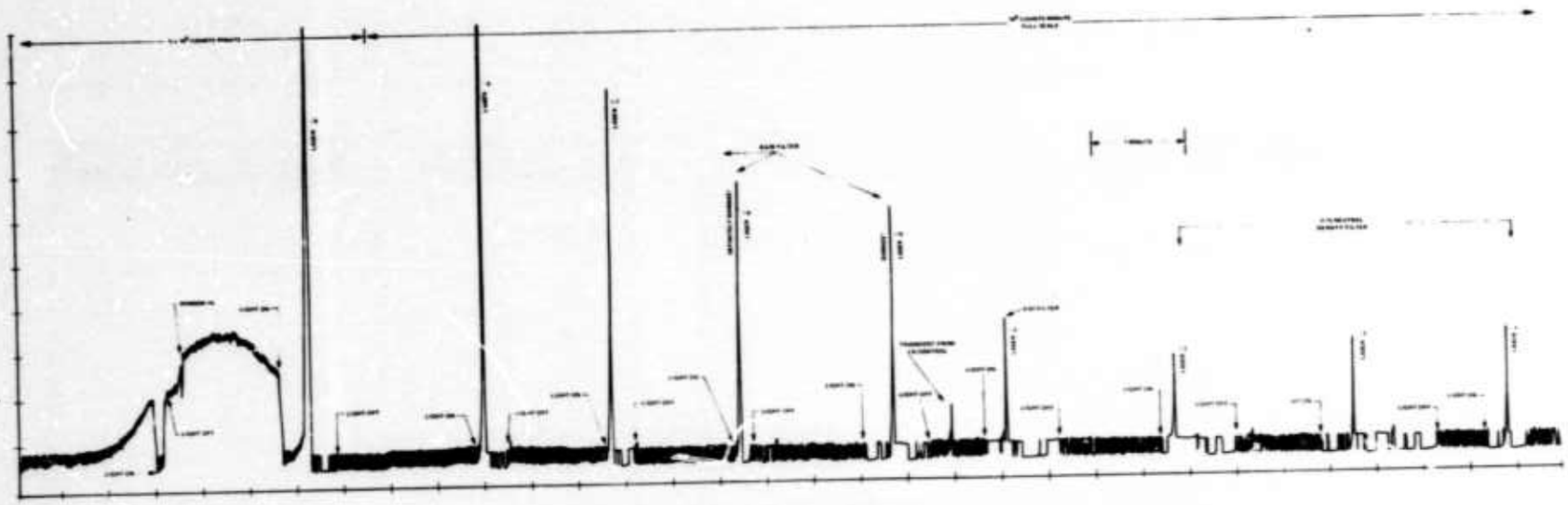

Figure 33 - OSEE after damage.

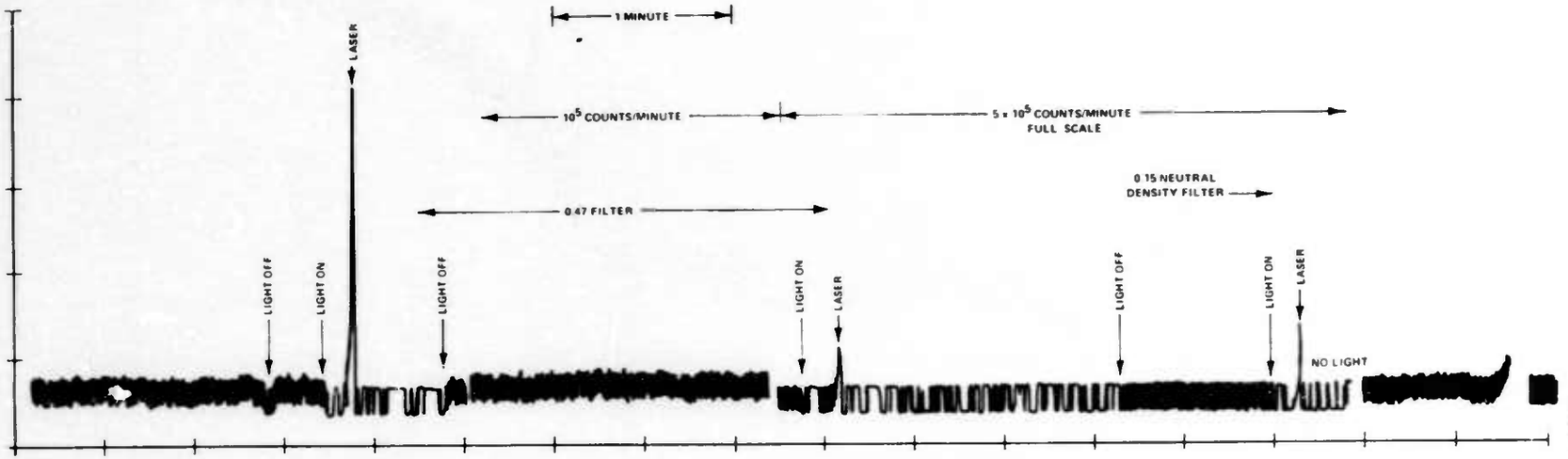

Figure 34 - OSEE from damaged spot after exposure to weak laser pulses.

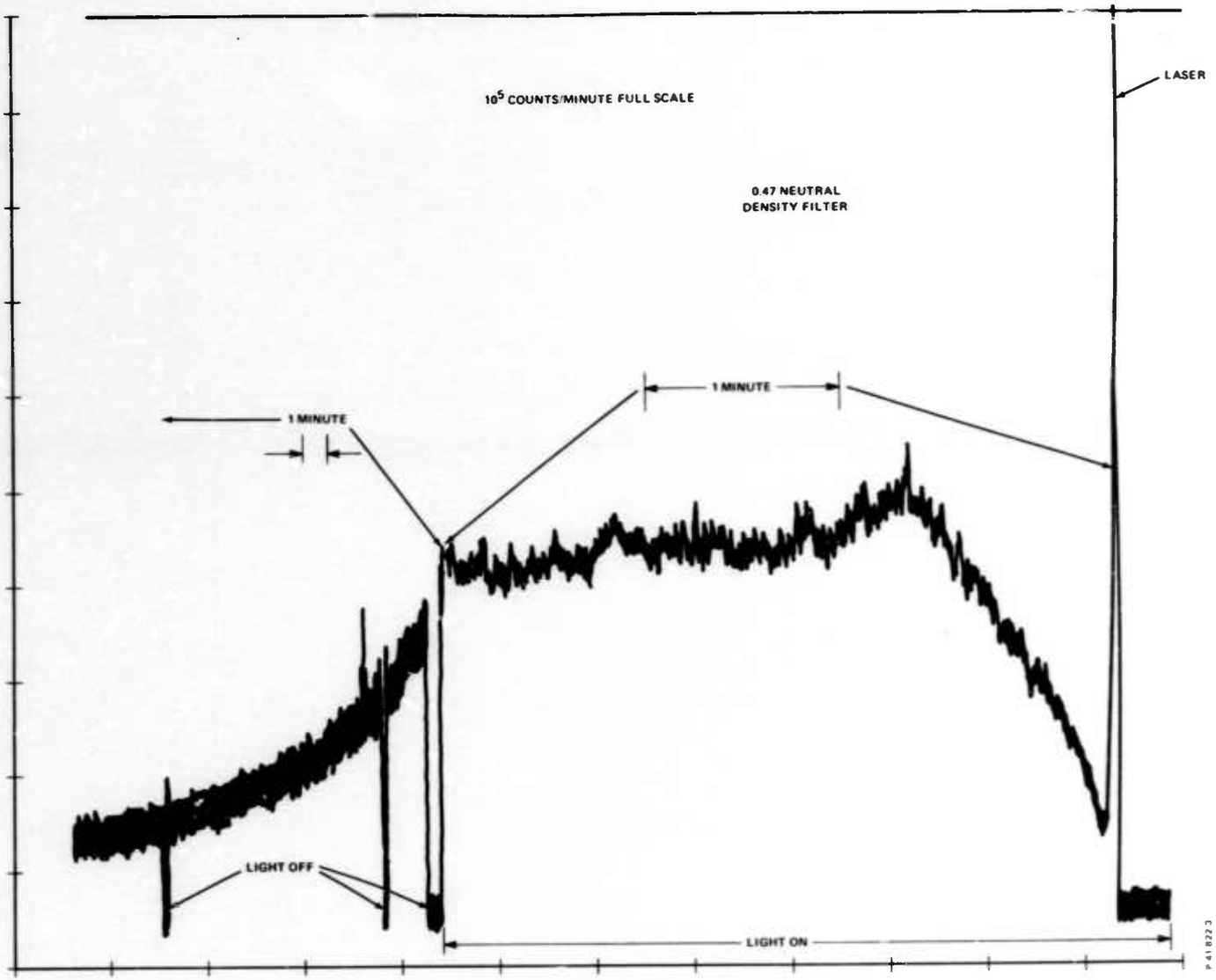

Figure 35 - Increased OSEE from damaged spot after exposure to weak laser pulses

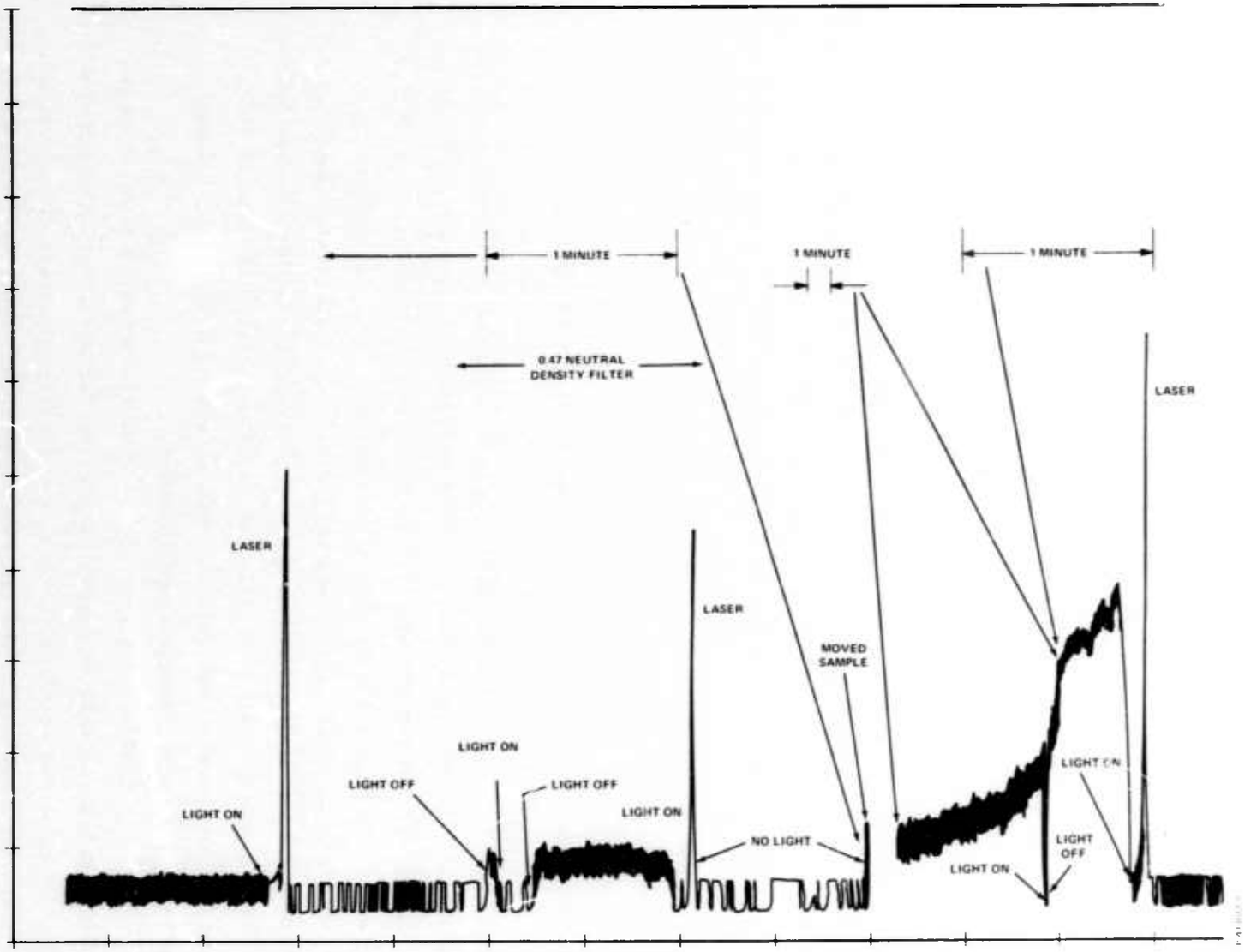

Figure 36 - More OSEE from the damaged spot (#1) and OSEE from a new spot (#2 and #3)

been left over from #1 shot; the fact that the emission after #3 shot (in Figure 36) is decreased supports this. The sample was then exposed at the same spot to two more shots attenuated with the 0.47 neutral density filter and then with one shot with less attenuation using the 0.70 filter. The emission each time was the same as that for #3 in Figure 29. However, the next shot (Figure 37) produced increased emission. More emission was produced with the pulse shown in Figure 38. The emission is seen to decrease and level off; the effect of attenuating the tungsten light by inserting a glass plate is also shown. We did not pursue this run further to determine where the emission decreased. Rather the spot was exposed to another laser pulse. The resulting OSEE began at the nominal background level, slowly increased, and leveled off after ~10 min. Again we did not measure its decay, but instead exposed the spot to further shots. OSEE from these latter shots peaked out within several minutes and then leveled off. Examples of some of these types of behavior are shown in Figure 39. The behavior of the OSEE in run #2 of Figure 39, in which the OSEE slowly increased from the nominal background level, is noticeably different from the OSEE shown in Figures 37 and 38. In Figures 37 and 38, the OSEE increased from one shot to the next; within a single run, it slowly decayed after lamp illumination rather than slowly increasing. A more recent example of the Figures 37-38 behavior is shown in Figures 40 (#3 and #4) and 41. Emission was still observed after 1.5 hr (see #4 in Figure 40) of lamp illumination! Also, in evidence was the increase in laser signal peak height and peak tail development which occurred as the sample spot was exposed to consecutive laser pulses having sufficient power density to cause damage (Figure 33). In some of these runs, charge emission was detected when no visual evidence of a damage spark or no apparent damage could be found.

Finally, in Figure 42, we show the emission after exposure to laser pulses capable of sample damage for the situation in which the detector input was biased at a -3300 V retarding potential for electrons. Although the laser signal and post-emission occur, there was no clear evidence of OSEE.

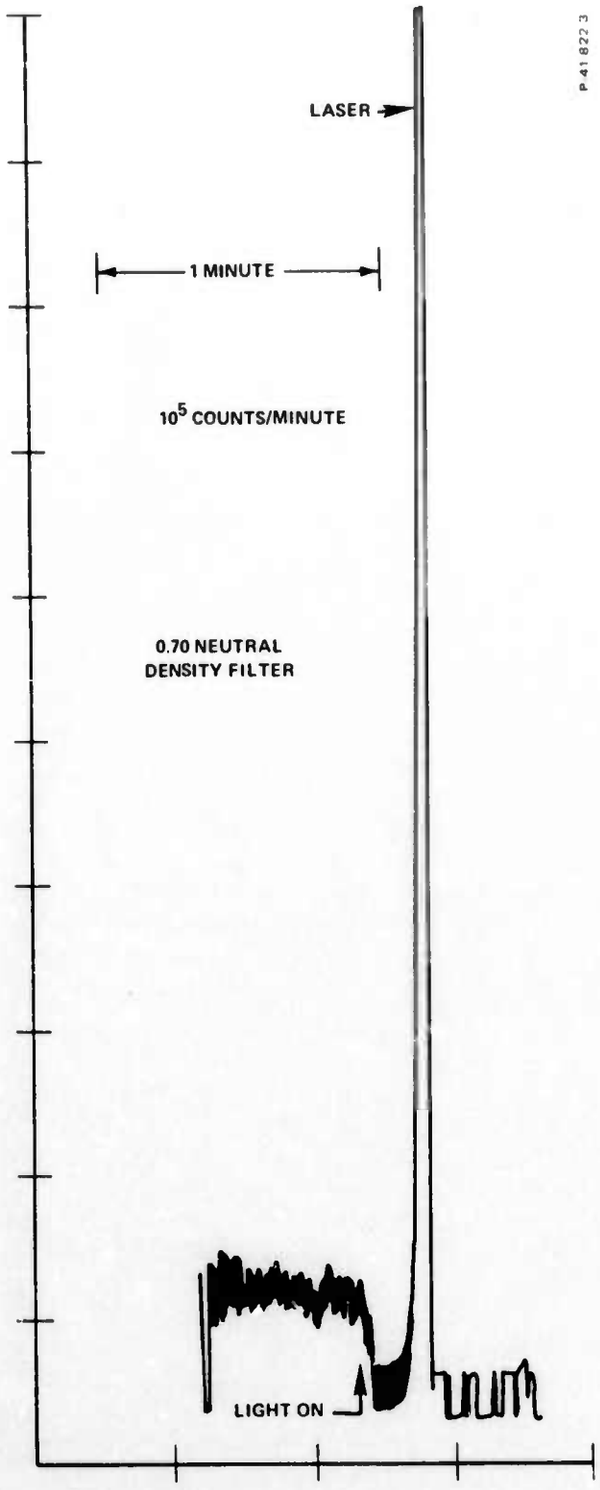

Figure 37 - Increased OSEE from new spot

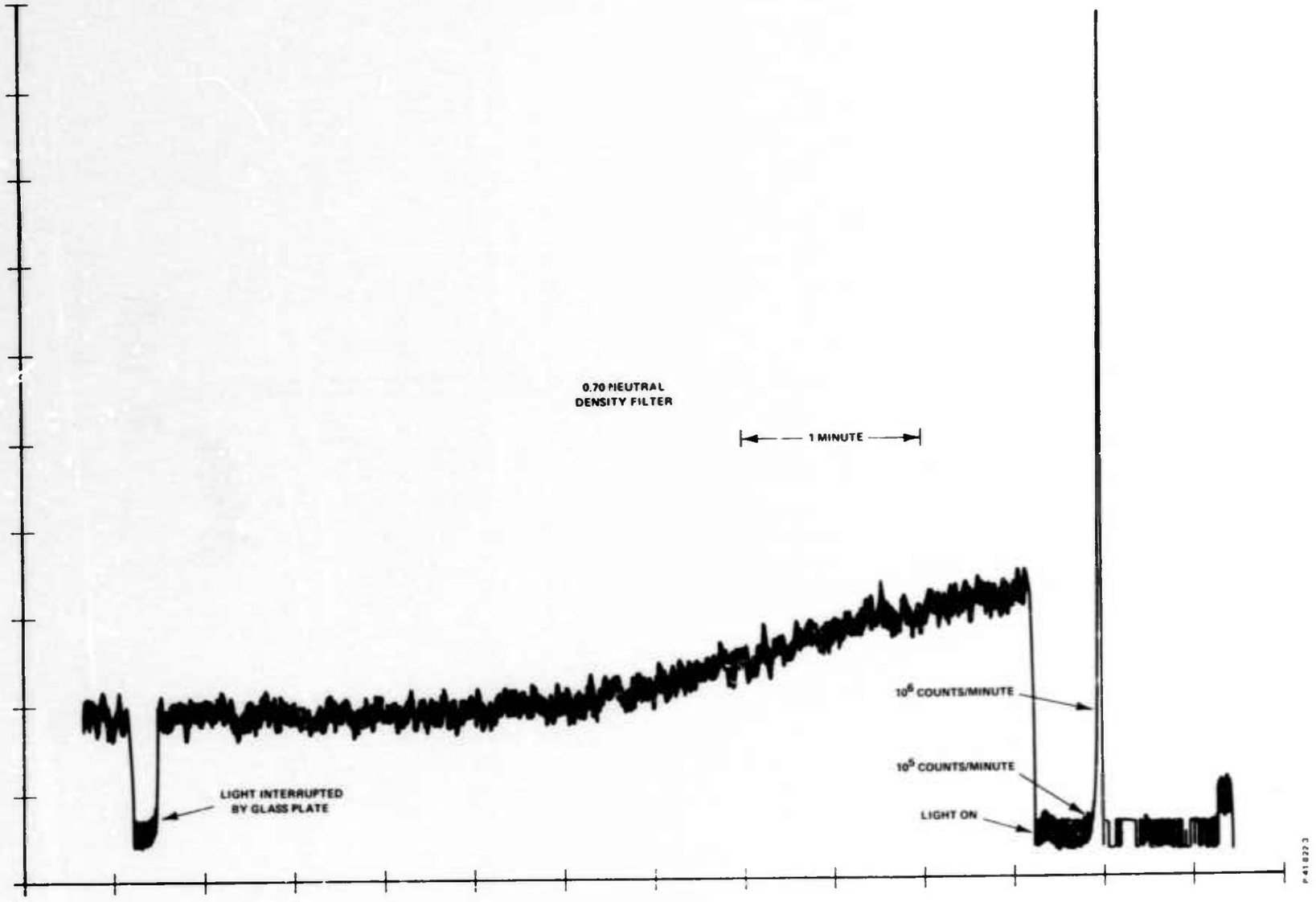

Figure 38 - Further OSEE from new spot

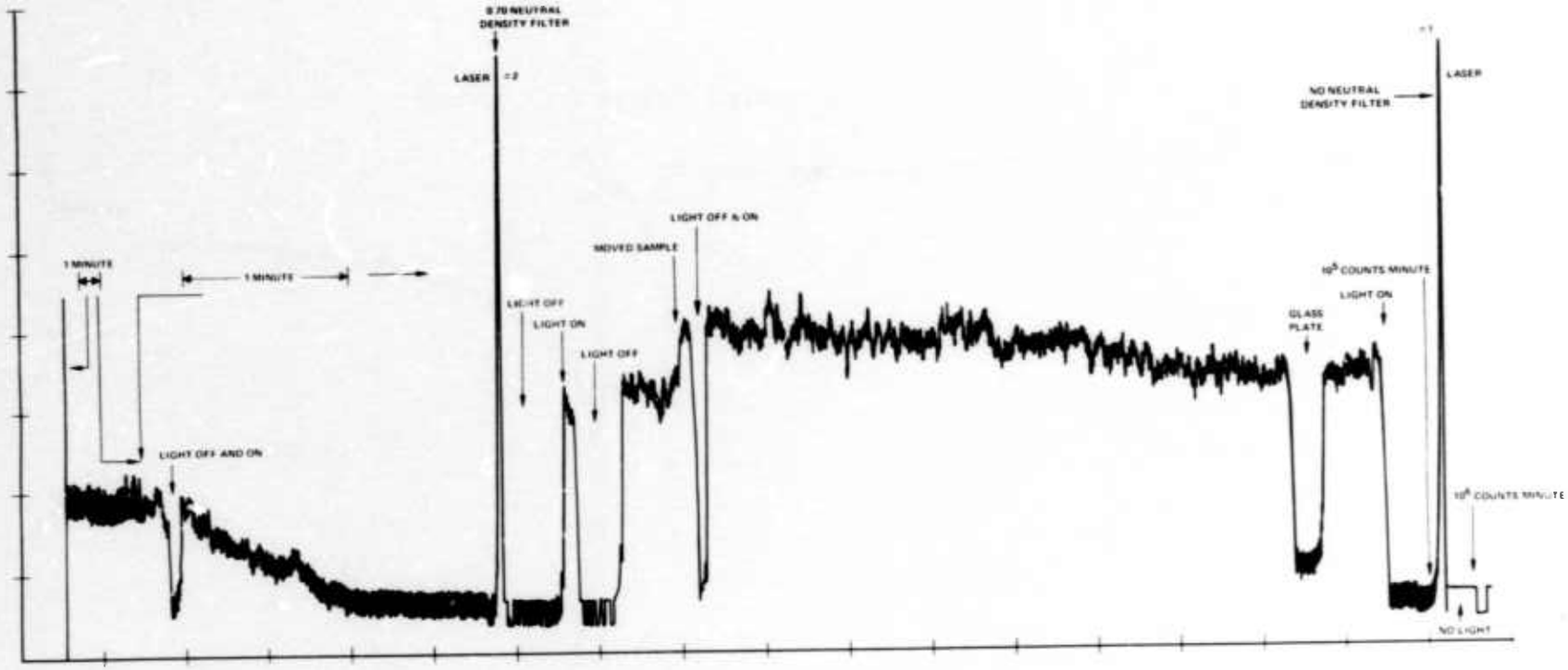

Figure 39 - Example of the OSEE increasing and leveling off.

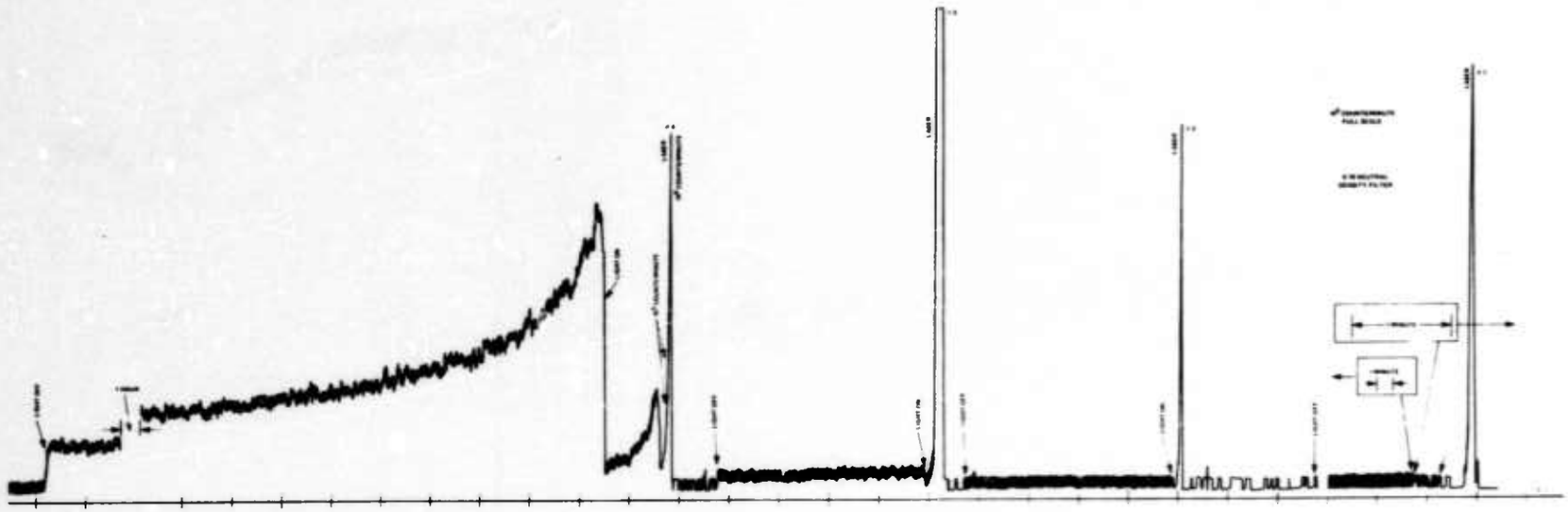

Figure 40 - Another sample of OSEE after damage.

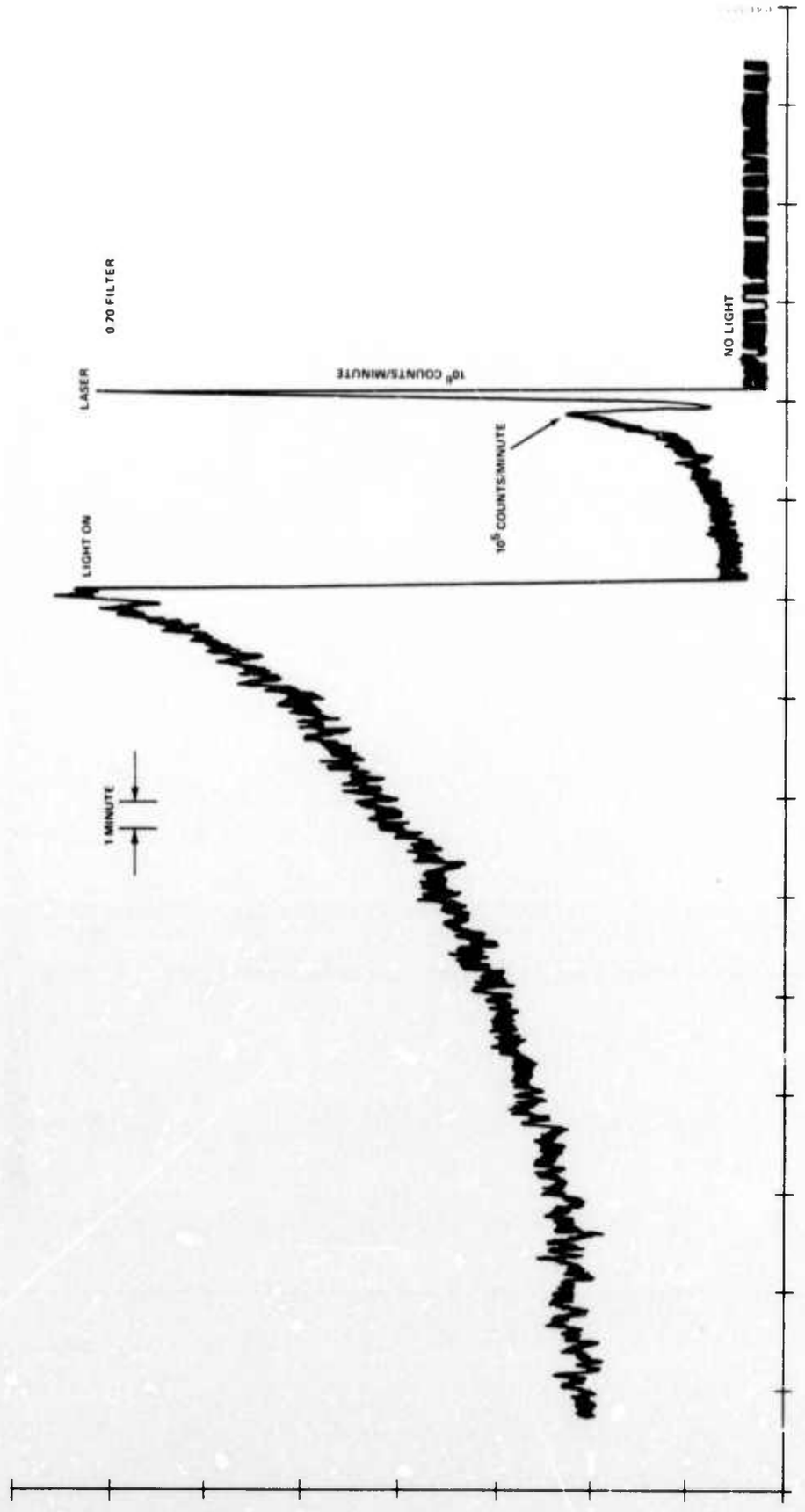

Figure 41 - Further OSEE after damage

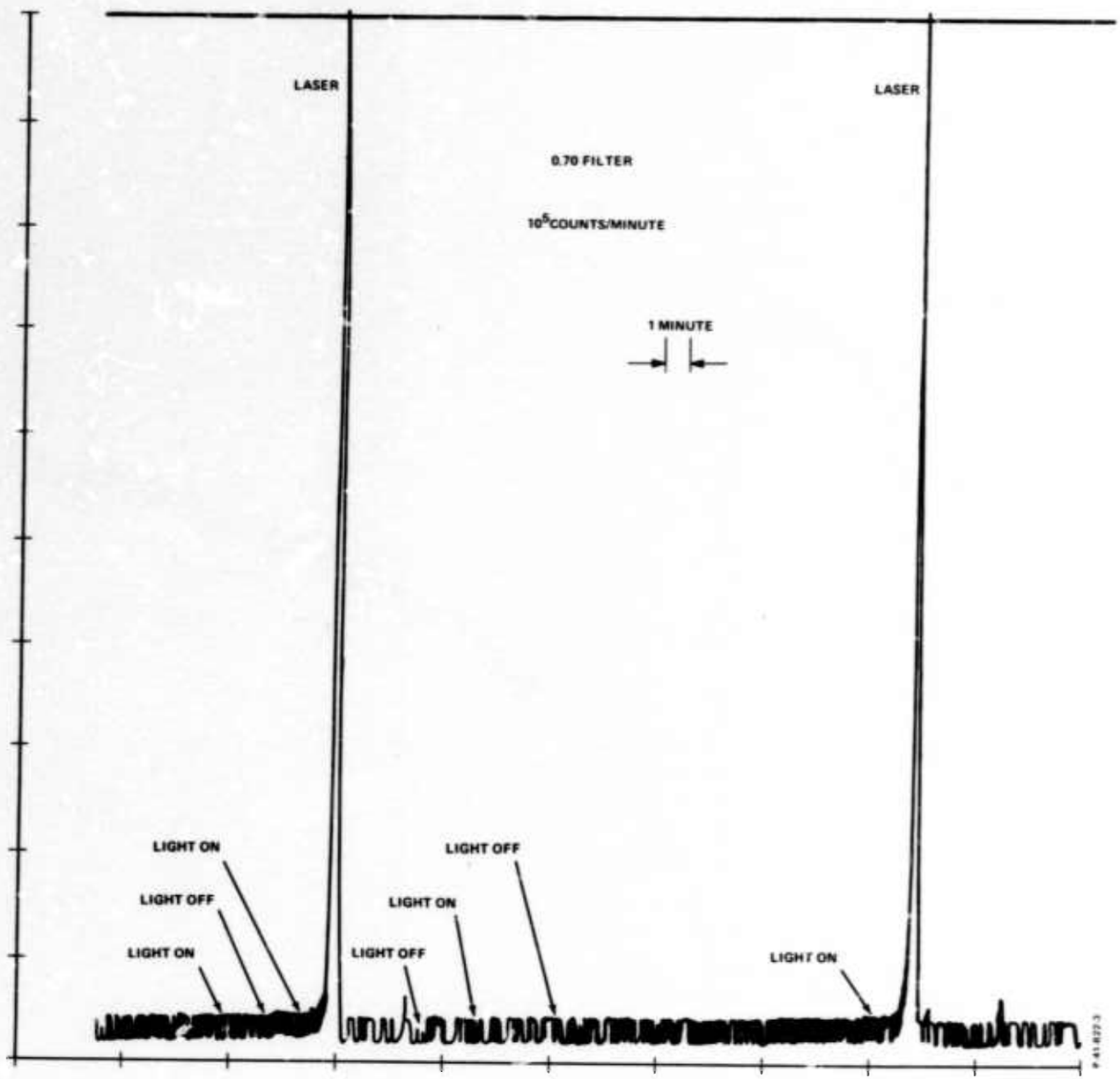

Figure 42 - Detected emission with a -3300 V retarding potential

4.2.3 Discussion

The results of our investigations of OSEE from $LiNbO_3$ show a wide range of variation in the emission pattern for constant and for different operating conditions. Attempts to correlate the observed differences with changes in the operating parameters have not been successful. Most likely, this lack of success was caused by changes in surface conditions of the sample - changes which we are not yet able to control or measure. In the OSEE studies of surfaces bombarded by electrons, the varying effects are most likely due to a combination of surface structure and charging phenomena. The appearance of the "second" peak is most curious, particularly in light of the long delay time involved; it may well be due to a different mechanism than the first peak. One possibility is a barrier effect, caused by surface charging, which prevented trap emptying until the barrier decayed to some low level. Also, we have not been able to ascertain the role, if any, of the crystal polarization. Our concern was that local heating at the crystal surface, caused by the lamp illumination and surface imperfections, may have produced thermally stimulated field emission. However, this does not appear to be the case because similar emission effects are observed on both the c^+ and c^- surfaces and because the emission responds rapidly to interruptions of the lamp illumination, especially cut off. More convincingly, no emission peaks were observed without previous electron bombardment of exposure to laser pulses.

Similarly, we have not yet successfully correlated the observed emission after laser exposure with changes in the operating conditions. Again, we feel that the surface conditions were changing. Our concern in the laser work is whether surface damage is a prerequisite for OSEE in $LiNbO_3$. Although some of our experimental results indicate that damage is not required, further experimental work involving a higher degree of apparatus sophistication than presently available will be necessary to substantiate this possibility.

Further experimental work to unravel the reported effects should proceed along the lines of increased control over the surface

conditions, possibly through use of ultrahigh vacuum techniques for surface preparation and characterization. It will also be necessary to monitor the surface during and after trap excitation in order to detect changes. Until this sophistication is adopted, it does not appear worthwhile to continue the OSEE investigations.

SECTION 5
EXOELECTRON EMISSION MICROSCOPE

An electrostatic exoelectron emission microscope was described in the previous semi-annual report. Testing of this microscope had just begun at that time. Further testing revealed several design deficiencies which were responsible for the failure of the microscope to operate. Electrode misalignment and insulation problems were the main causes of this failure. A new lens design was thus initiated to correct these problems.

The electrode mount was the only part of the microscope requiring a change in design. As described in the first semi-annual report, the lens structure moves in a high-precision oil-free bearing race. It was decided that additional adjustment flexibility would be worthwhile. A gimbal-type mount with three fine-threaded screws was developed. This structure, which is shown in Figure 43, is commonly used in optical systems. It provides for fast adjustment of the lens with respect to the optical axis.

The new electrodes were machined from brass, then polished and gold-plated. The insulators in the vicinity of the transmitted electron beam were suitably shielded to prevent surface charging.

The lens configuration was changed from a three-electrode structure to an immersion objective of the Brüchi type; two electrodes are employed. Extensive work on this lens has been reported in the literature.[14] According to Recknagel,[15] the resolution of this lens depends mainly on the field strength close to the emitting surface; the thinner the first electrode, the higher the field strength. In practice, however, the thickness cannot exceed some minimum value which is set by structural requirements. These requirements are particularly stringent when the sample is heated. Therefore, we chose a thickness of 0.030 in. for both electrodes. Moreover, an increased field strength is obtained by moving the second electrode

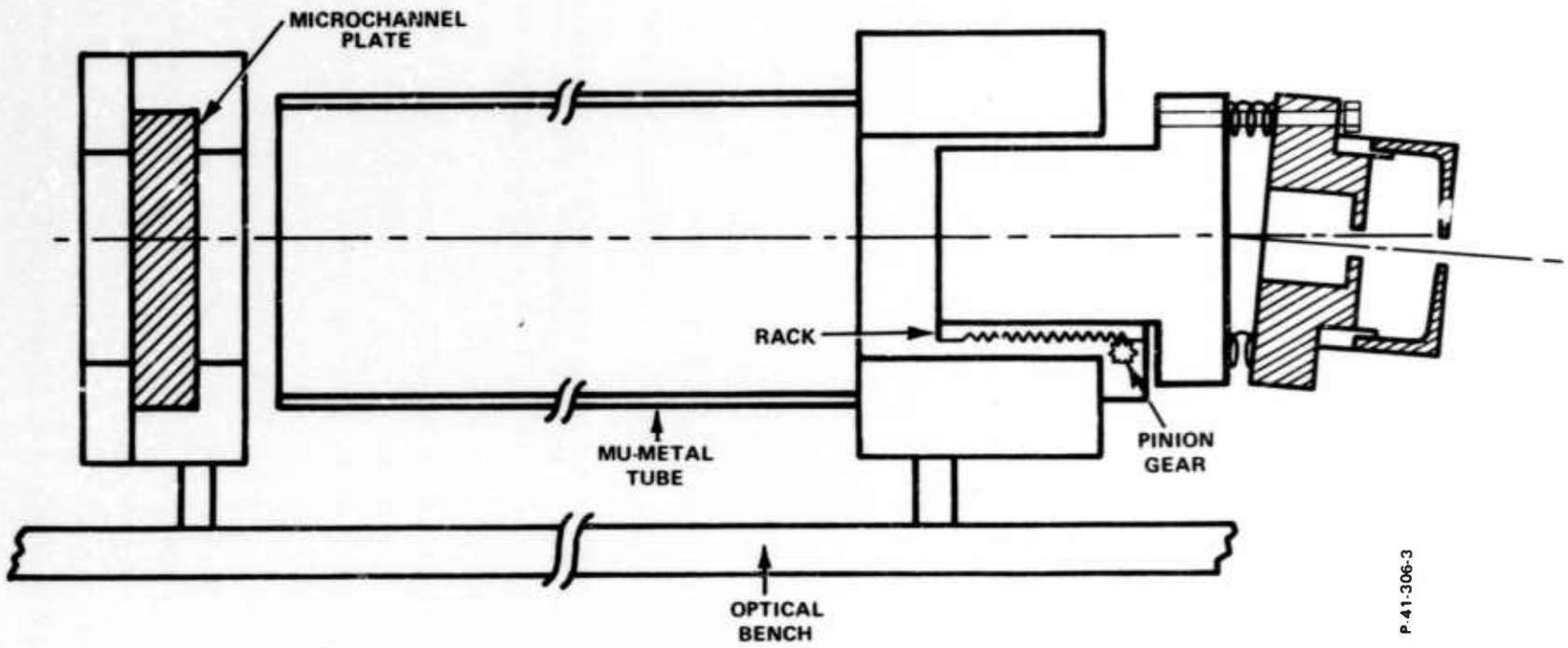

Figure 43 - Schematic of the exoelectron microscope

(anode) closer to the emitting surface. Insulation breakdown however limits the distance between the first and second electrodes. We thus used a separation of 0.040 in. which is adequate for operating voltages up to 2.5 keV.

SECTION 6
FUTURE WORK

The research results, described in the previous sections, have not only affected the scope of this present contract but have also shown that more work is required than originally anticipated to understand the physical processes that lead to exoelectron images on, and ultimately catostrophic failure of, a sample surface upon exposure to intense laser beams. We propose therefore the following work statement:

(a) Continue theoretical anlysis of the physical processes that lead to exoelectron emission from alkali halides after exposure to intense laser light; in particular, include the temperature effects in the calculation and discuss the possible involvement of a rapid rise in temperature in the damage mechanism.

(b) Perform experiments that are designed to elucidate the physical processes which lead to exoelectron emission and, at high laser powers, to the failure of the samples; in particular, study nominally pure NaCl that is exposed to ruby laser pulses.

(c) Analyze the results of both the experiments and the theoretical calculation with respect to the feasibility of using exoelectron techniques as a NDT method for laser surface damage.

SECTION 7

ACKNOWLEDGEMENTS

We are indebted to Dr. N. Boling for the use of the Owens-Illinois Nd-glass laser. A. Schmidt contributed to the experimental effort. The participation of Dr. P. Kelly, National Research Council, Ottawa, Canada, in the work is gratefully acknowledged. As a result of his earlier collaboration, computer programs to solve the rate equations of electron kinetics in solids were available.[6,7] He modified these programs appropriately and performed all numerical computer calculations.

SECTION 8

REFERENCES

1. P. Bräunlich, Appl. Phys. Lett., 20, 4 (1972).
2. J. J. Markham, "F-Centers in Alkali Halides," Solid State Physics Supplement 8, F. Seitz ed. (Academic Press, New York, 1966).
3. I. M. Catalano, A. Cingolani, and A. Minafra, Phys. Rev. B5 1629 (1972).
4. V. S. Dneprovkii, D. N. Klyshko, and A. N. Penin, Sov. Phys. JETP Lett., 8, 103 (1966).

   (We used the smaller value of the cross section cited by Catalano et al., in order not to overestimate 5-photon effects which are neglected by Bloembergen's group[8] but, nevertheless, seem to play an important role in the process discussed in this report.)
5. D. H. Kleinman, Phys. Rev., 125, 87 (1962).
6. P. Kelly and P. Bräunlich, Phys. Rev., B1, 1587 (1970).
7. P. Kelly, M. J. Laubitz, and P. Bräunlich, Phys. Rev., B4, 1960 (1971).
8. Yu. P. Raizer, Sov. Phys. USPEKHI, 8, 650 (1966).
9. Eli Yablonovitch and N. Bloembergen, Phys. Rev. Lett., 29, 907 (1972).
10. D. W. Fradin and M. Bass, Appl. Phys. Lett., 22, 206 (1973).
11. R. W. Hellwarth, N.B.S. Special Publication, 341, 67 (1970).
12. D. W. Fradin, N. Bloembergen, and J. P. Letellier, Appl. Phys. Lett., 22, 635 (1973).
13. G. A. Vorobev, N. I. Lebedeva, and G. S. Nadorova, Sov. Phys. Solid State, 13, 736 (1971).
14. E. Hahn, Optik 15, 500 (1958); Optik 16, 513 (1959); A. Septier, Annal. Radioelectr. 9, 374 (1954); E. A. Soa, Jenaer Jahrbuch, I, 115 (1959).
15. A. Recknagel, Z. Phys. 120, 331 (1943).

SECTION 9
SUMMARY

This is the second semi-annual report for a program that is directed toward the development of a nondestructive method to predict laser surface damage of transparent dielectric materials used in high power laser systems. The test program includes (1) investigation of exoelectron properties of a series of selected laser optical materials after exposure to ionizing radiation or to high peak power laser pulses, (2) correlation of exoelectron images, obtained after exposure of the surface to laser pulses, with the laser surface damage characteristics of these surfaces, and (3) study of the feasibility of using exoelectron surface imaging as a technique to nondestructively predict the laser surface damage threshold of laser optical materials.

During the reporting period we have studied thermally stimulated exoelectron emission from Nd-2 laser glass and NaCl single crystals after electron bombardment and optically stimulated exoelectron emission from NaCl and $LiNbO_3$ single crystals. Several new phenomena were discovered.

Important new results were obtained on the mechanism of exoelectron imaging on LiF surfaces. Computer calculations of the spatial variation of the density of trapped electrons after exposure of the sample (e.g., NaCl) to a TEM_{00} mode laser beam lead us to conclude that the multiphoton processes cannot be responsible for the exoelectron images observed, e.g., on LiF at the relatively low laser power densities used in these experiments. The occurrence of a white-hot plasma in front of the examined surfaces was found to be the necessary condition for the observation of the characteristic exoelectron images at these power densities. However, this is not to say that multiphoton processes do not occur or are not dominant at higher laser powers. On the contrary, according to our calculations, at power densities approaching the so-called dielectric breakdown threshold as measured by Bloembergen's

group, multiphoton photocarrier generation and free carrier absorption will indeed produce the characteristic exoelectron image in the absence of any hot plasma. As a further result, a rapid rise in the temperature of the sample during laser exposure (due to free carrier absorption) may conceivably contribute to catastrophic failure of the optical material. More detailed calculations and carefully designed experiments are expected to provide important new insight into the exoelectron processes and the mechanism of laser damage in optical materials.